

Project SANC

Support of Analytic and Numeric Calculations for experiments at Colliders (project within JINR theme 02-0-1062-2002/2014 and after 2014 year within JINR theme 02-0-1081-2009/2019)

D.Yu. Bardin¹, P.Ch. Christova², L.V. Kalinovskaya, V.A. Kolesnikov, L.A. Rumyantsev,
R.R. Sadykov, A.A. Sapronov, E.D. Uglov — NEOVP, DLNP, JINR, Dubna, Russia;
A.B. Arbuzov, S.G. Bondarenko — BLTP, JINR, Dubna, Russia;
W. von Schlippe — PNPI, RAN, Gatchina, 188300, Russia;
T. Riemann — DESY, Zeuthen, Germany;
G. Nanava — Scientific Computing Team Leader, Leibniz Universitat, Hannover, Germany;
Z. Was — IFJ, PAN, Krakow, Poland;
Lucia Di Ciaccio — ATLAS group of LAPP, Laboratoire d'Annecy-le-Vieux de physique
des particules (LAPP), Annecy;
U. Klein, A. Glazov, J. Kretzschmar — CERN, DESY and University of Liverpool,
England.

¹deceased

²deceased

Contents

1	Introduction	3
2	SANC tree	5
2.1	Basic notions: precomputation, amplitudes, form factors...	5
2.2	From analytic results to numbers	6
2.3	Types of SANC Output	6
3	SANC application for selected processes	8
3.1	$t \rightarrow bl\nu$ decay	8
3.2	$f_1\bar{f}_1 \rightarrow ZZ$	8
3.3	Three channels of $f_1\bar{f}_1HA \rightarrow 0$	8
3.3.1	Annihilation channel $f_1\bar{f}_1 \rightarrow HA$	9
3.3.2	Decay channel $H \rightarrow \mu^+\mu^-\gamma$	10
3.3.3	Production channel $e\gamma \rightarrow eH$	10
3.4	Three channels of $f_1\bar{f}_1ZA \rightarrow 0$	11
3.5	Two channels of $\bar{f}_1f_1HZ \rightarrow 0$	11
3.5.1	Covariant amplitude of the process	12
3.5.2	Annihilation channel $e^+e^- \rightarrow HZ$	12
3.5.3	Decay channel $H \rightarrow Zf_1\bar{f}_1(\gamma)$	12
3.5.4	$H \rightarrow Zf_1\bar{f}_1$: a MC generator for $H \rightarrow 4\mu$ decay	12
3.5.5	MC $H \rightarrow 4\mu$: Prophecy4f & SANC comparison	13
3.6	Drell-Yan-like W and Z production	13
3.6.1	CC and NC Drell-Yan processes distributions	14
3.6.2	QCD-EW interplay	16
3.6.3	Light pair corrections to Drell-Yan processes	17
3.7	4-boson study: $\gamma\gamma \rightarrow \gamma\gamma$, $\gamma\gamma \rightarrow \gamma Z$, $Z \rightarrow \gamma\gamma\gamma$, $\gamma\gamma \rightarrow ZZ$	17
3.8	Auxiliary J functions	20
4	SANC, application to ATLAS	21
4.1	MCSANC integrator	21
4.2	Electroweak corrections for ATLAS Drell-Yan analysis	24
4.3	Drell-Yan processes: tuned comparison	27
5	QCD analysis and XFitter (HERAFitter) development	29
6	The main objectives of the SANC group in 2018 year	35
7	Conclusion	35

1 Introduction

This report summarises the scientific activity within the **SANC** project (Support of Analytic and Numeric Calculations for experiments at Colliders) from 2001 to 2018.

The research area of this project spanned over LHC physics and hadron collision phenomenology, fixed order radiative corrections to the Drell–Yan processes, QCD-analysis of experimental data and DGLAP formalism. The results obtained by the participants have been presented in 73 publications in peer-reviewed journals and reported at international workshops and conferences.

Precision tests of the Standard Model (SM) at LHC nowadays become more and more important. The accuracy of the corresponding experimental studies grows up continuously with collected statistics, improved detector calibration, elaboration of analysis techniques etc. All that leads to new requirements on the accuracy of theoretical predictions challenged by the experimental data.

The **SANC** project roots back to early 2001. It was announced first in Ref. [1] and its first phase status report was presented at ACAT2002 in several talks [2]–[3].

The main prerequisites for the studies undertaken were the expertise of the participants in the field of collider phenomenology and data analysis, long history of development of theoretical basis and instruments, access to the newest experimental results and active collaboration with the international scientific community.

The main aim of the project is the creation of a computer system for semi-automatic calculations of realistic and pseudo-observables for various processes of elementary particle interactions “from the SM Lagrangian to event distributions” at the one-loop precision level for the present and future colliders – TEVATRON, LHC, electron Linear Colliders (ISCLC, CLIC), muon factories etc.

Computer-wise, **SANC** is an IDE (Integrated Development Environment) and is realized as a server–client application. **SANC** client for version v.1.10 can be downloaded from servers at CERN <http://pcphysanc.cern.ch/> and Dubna <http://sanc.jinr.ru/>.

Physics-wise, all the calculations at the one-loop precision level are realized in the spirit of the book [4] in the R_ξ gauge and all the results are reduced up to the scalar Passarino–Veltman functions: A_0 , B_0 , C_0 , D_0 . These two distinctive features allow to perform several checks: e.g. to test gauge invariance by checking the cancellation of gauge parameter dependence, to test various symmetry properties and validity of various Ward identities, all at the level of analytical expressions. The process of calculation is structured into several well-defined steps. With the help of the **SANC** system it is easy to follow all steps of calculations for many SM decays and processes. This makes the **SANC** system particularly appealing for educational purposes.

The **SANC** system uses several computer languages, but only FORM for analytic calculations [5]. All codes are put in a special program environment, written in JAVA. At early phase it was used for a revision of atomic parity violation [6], for a calculation of one-loop electroweak radiative corrections for the processes $e^+e^- \rightarrow f\bar{f}$ [7] and neutrino DIS [8]. Meantime, in Ref. [9] it was used for precision comparison of EW corrections for the SM boson decays into fermion-antifermion pairs and in [10] for an improvement of the PHOTOS Monte Carlo generator.

In the second phase of the project (2004–2010), the calculations were extended to a large

number of HEP processes, with an emphasis on LHC physics. In Ref. [11] we have summarized the status of the **SANC** version 1.00, in which we implemented theoretical predictions for many high energy interactions of fundamental particles at the one-loop precision level for up to 4-particle processes. In that paper we placed an emphasis on an extensive discussion of the “Precomputation procedure”, an important first step of calculations of the one-loop amplitudes for 3- and 4-particle processes in QED, QCD and EW theories. Finally, in Ref. [12] we described **SANC** version 1.10 upgraded both physics-wise and computer-wise compared to version 1.00. As far as physics is concerned it contains an upgraded treatment of $u\bar{d} \rightarrow l^+\nu_l$ and $d\bar{u} \rightarrow l^-\bar{\nu}_l$ processes used for precision calculations of Drell–Yan processes (see Ref. [13]) and a complete implementation of $t \rightarrow b + l^+ + \nu_l$ CC decays up to numbers and MC generators [14, 15]. We also implemented several processes like $f_1\bar{f}_1ZZ \rightarrow 0$ and $f_1\bar{f}_1HZ \rightarrow 0$, and the process $H \rightarrow f_1\bar{f}_1A$ in three cross channels [16] in the EW branch, $\gamma\gamma \rightarrow \gamma\gamma$ scattering [17] and $ll \rightarrow \gamma\gamma^*$ in the QED branch, as well as a new QCD branch [18], [19]. Starting from Ref. [12] we use a generalized approach: we begin with a presentation of the covariant amplitudes for a process, say $f_1\bar{f}_1HZ \rightarrow 0$, where $\rightarrow 0$ means that all 4-momenta flow inwards. The derived scalar form factors can be used for any physically sensible cross channel (here two: annihilation $f_1\bar{f}_1 \rightarrow HZ$ and decay $H \rightarrow Zf_1\bar{f}_1$, since it is known that $M_H > M_Z$) after an appropriate permutation of their arguments (s, t, u). Then we compute helicity amplitudes for every cross channel separately. In the same spirit we considered the three channels of the process $f_1\bar{f}_1ZA \rightarrow 0$ [20].

The third phase (2010–2018) was mostly devoted to physical applications of **SANC** Monte Carlo Integrators and Generators based on the above mentioned modules. Meantime, modules for several more processes were implemented in the **SANC** framework: top quark decays, QCD corrections to Drell–Yan [21],[22],[23], 4-boson processes ([24], [25] and [26]) and single top quark production. Drell–Yan-like processes [27], i.e. single Z and W boson production with subsequent decay into a lepton pair [28],[29], provide at LHC the ultimate benchmark in the experimental precision. The theoretical description of these processes within the SM is constructed taking into account various possible effects including radiative corrections, PDF uncertainties and scale variation. DY analysis for LHC by the **MCSANC** integrator – [28], [30], [31], [32] and also ATLAS note ATL-PHYS-INT-2011-081 and [33], [34], [35].

Within the **SANC** framework we have also computed one-loop QED radiative corrections to high-energy lepton bremsstrahlung on heavy nuclei [?].

Tuned comparisons between independent results of several ATLAS research groups show a perfect agreement in description of QCD and electroweak radiative corrections in the one-loop (NLO) approximation. Higher order effects are also shown to be important to provide the required accuracy level: [36], [37], [38]. It has been extensively verified and cross checked against similar instruments and was proven to provide a reliable advanced cross section predictions at both parton and hadron levels. At tree level we compared with GRACE-tree [39], CompHEP [40], PHOTOS [41]–[42], PYTHIA [43] whereas one-loop level results were checked against HORACE [44]–[45], WGRAD2 [46]–[47], ZGRAD2 [48]–[49], a code by S. Dittmaier and M. Kramer [50], FeynArts [51]–[52] and GRACE-loop [53].

2 SANC tree

The SANC system deals with the three models of elementary particle interactions – QED, EW and QCD. In Fig. 1 we show processes only for the EW branch.

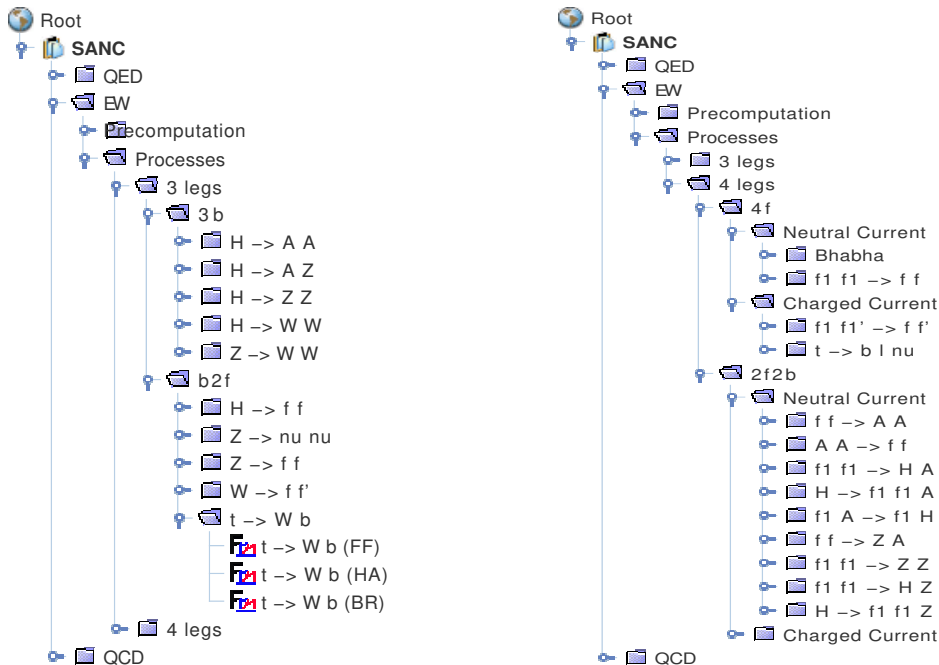


Figure 1: Three and four particle EW processes available in SANC version 1.10

Each tree consists of several levels of “folders” which end up with “files”, normally three: FF (Form Factors), HA (Helicity Amplitudes) and BR (Bremsstrahlung). For labels of folders we use notations: b for any boson; $f(f_1)$ for any fermion (f_1 for massless fermions of the first generation whose mass is kept only in arguments of logarithmic functions); A, Z, W, H for photon and Z, W, H bosons; the same holds for files but with t, b meaning top and bottom quarks, respectively.

For many processes the SANC calculations end up with MC integrators or event generators. But only few of them are embedded into the system itself, see Ref. [3]. The other codes are accessible as stand-alone ones. The latter widely use FORTRAN modules generated by the system (see below).

2.1 Basic notions: precomputation, amplitudes, form factors...

Precomputation is one of important concept of SANC ideology. Since many one-loop calculations are enormously time consuming, the idea is to precompute as many one-loop diagrams and derived quantities (renormalization constants, etc) as possible. The precomputation trees are presented and exhaustively discussed in the Ref. [11] and we refer the reader to this paper.

As seen from an open folder for $t \rightarrow Wb$ decay in the Fig. 1, one has usually three files written in FORM, which compute:

- Covariant amplitude (CA) and scalar FF, cf. with the nucleon-nucleon- γ vertex parametrized by the two scalar FF $\mathcal{F}_{1,2}$: $\mathcal{A} \propto \gamma_\mu \mathcal{F}_1 + \sigma_{\mu\nu} q_\nu \mathcal{F}_2$;
- HA, which depend on FF, $\mathcal{H}_{\{\lambda_i\}}(\mathcal{F}_i)$, where $\{\lambda_i\}$ denotes a set of helicity quantum eigenvalues, typically spin projections onto a quantization axis. We remind that in the standard approach for an observable O one has: $O \propto |\mathcal{A}|^2$, while in terms of HA: $O \propto \sum_{\{\lambda_i\}} |\mathcal{H}_{\{\lambda_i\}}|^2$ and this drastically simplifies calculations since $\mathcal{H}_{\{\lambda_i\}}$ are scalar objects which are computed as complex numbers. Many other examples of CA and HA may be found in Refs. [11], [12] and [16];
- Accompanying real BR. This module computes the contribution of the real bremsstrahlung to a relevant process. Typically we have both the calculations of inclusive quantities and fully differential ones for a use in the MC codes.

2.2 From analytic results to numbers

The chain of **SANC** calculations starts with on-line execution of module FF, followed by an **s2n** run (see short User Guide at our Project home pages, indicated in the Introduction), and subsequent execution of module HA with another **s2n** run. As the result, the system generates a FORTRAN code for the contribution of virtual corrections to a chosen process in the following schematic form:

$$d\Gamma(d\sigma) \sim \sum_{\lambda_i \lambda_j \lambda_k \lambda_l} \left| \mathcal{H} \left(\mathcal{F}^{\text{Born}+1\text{loop}+2\text{loop}} \right)_{\lambda_i \lambda_j \lambda_k \lambda_l} \right|^2. \quad (1)$$

Note, that the 2-loop corrections may be easily embedded into this scheme if available.

Real corrections consists of Soft and Hard bremsstrahlung. They are computed by modules BR. The Soft has the Born-like kinematics, while Hard has + 1 particle's more phase space and typically the system creates a FORTRAN module which is used in subsequent MC calculations. For several processes, the system may compute complete one-loop corrections, including real bremsstrahlung for an inclusive observable.

For numerical computations we use the FORTRAN modules generated by the package **s2n** — a part of the system written in PERL. **SANC** includes its own FORTRAN library for numerical calculation of Passarino–Veltman functions and uses LoopTools as an alternative.

2.3 Types of SANC Output

Typical **SANC** outputs are:

- FORTRAN modules. These modules may be used in MC integrators and generators by ourselves or by the others;
- Standalone MC generators. As example we will present below some result obtained with:
 - a) generator for $t \rightarrow b l \nu$ decay;
 - b) generators for NC and CC Drell–Yan processes;
 - c) generator for $H \rightarrow 4\mu$ decay in the single Z pole approximation;
 - d) MCSANC integrator.
- Contribution to tuned comparison. We participated in three workshops: Les Houches

Workshop, see Proceedings 2006 [36], TEVATRON for LHC Report, 2007, [37], and Precision studies of observables in $pp \rightarrow W \rightarrow l\nu_l$ and $pp \rightarrow \gamma, Z \rightarrow l^+l^-$ processes at the LHC, see Report, 2017 [38].

3 SANC application for selected processes

In this section we present some recent results obtained with **SANC** for several selected processes: a) $t \rightarrow b\nu$ decay in QCD and EW sectors, [14],[54],[55],[56] and applications in LHC: [37]. b) $\bar{f}_1 f_1 \rightarrow ZZ$, [12],[56]; $\bar{f}_1 f_1 HA \rightarrow 0$: three cross channels, [16]; $\bar{f}_1 f_1 ZA \rightarrow 0$: three cross channels, [20]; $\bar{f}_1 f_1 HZ \rightarrow 0$: two cross channels, [12]; $H \rightarrow 4\mu$ decay, [12]; Drell-Yan-like W and Z production: [13], [23]; lepton pair emission corrections to Drell-Yan processes: [28],[29]. $\gamma\gamma \rightarrow \gamma\gamma$: [17],[24]; $\gamma\gamma Z\gamma \rightarrow 0$: two cross channels,[25]; $\gamma\gamma \rightarrow ZZ$, [26]; Auxiliary J functions in Passarino - Veltman reduction: [57],[58],[59].

3.1 $t \rightarrow b\nu$ decay

The results of this study are published in Ref. [14, 15, 54, 55, 56] We presented there: total width and various distributions; calculated without and with one-loop EW and QCD corrections; results of complete calculations and of the pole approximation; results obtained with MC integrator and event generator; comparison with world literature. As a typical result obtained with the MC event generator we show in Fig. 2 the complete EW correction $\delta = (d\Gamma^{\text{1loop}}/dM_{l\nu_l})/(d\Gamma^{\text{Born}}/dM_{l\nu_l}) - 1$, % as a function of invariant mass of $M = M_{l\nu_l}$ pair.

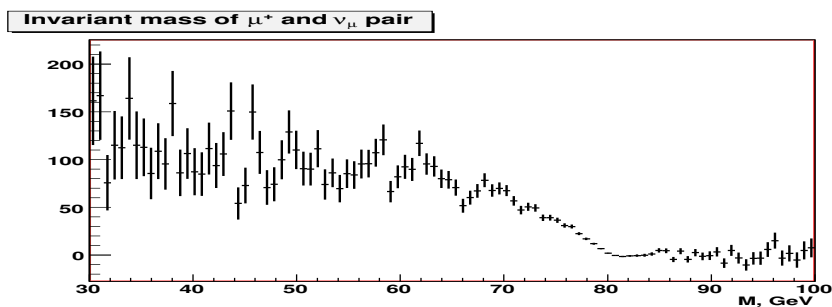


Figure 2: Complete EW correction δ (in %) as function of invariant mass of lepton pair $M_{l\nu_l}$

As seen from the Fig. 2, EW correction is very big below the resonance and rather small at and above resonance.

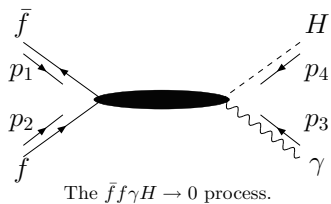
3.2 $f_1 \bar{f}_1 \rightarrow ZZ$

In Refs. [12, 56] we presented our analytic results for one-loop EW corrections for the process $f_1 \bar{f}_1 \rightarrow ZZ$. We found an excellent agreement with the numbers of Ref. [60]. In **SANC** we also have the hard photons contribution and the possibility to compute the hadron level process: $pp \rightarrow ZZ$.

3.3 Three channels of $f_1 \bar{f}_1 HA \rightarrow 0$

In the Ref. [16] we present the results of a unified approach when we begin with a common CA of all cross channels of process $f_1 \bar{f}_1 HA \rightarrow 0$, in which 4-momenta of external particles

are incoming:



For $f_1\bar{f}_1HA \rightarrow 0$ processes, the CA at one-loop order has the form:

$$\mathcal{A}^{\text{Born}+1\text{-loop}} = \mathcal{A}^{\text{Born}}[\mathcal{O}(m_f^2)] + \mathcal{A}^{1\text{-loop}}[\mathcal{O}(\alpha)] + \mathcal{A}^{1\text{-loop}}[\mathcal{O}(m_f^2\alpha)]. \quad (2)$$

The second term, $\mathcal{A}^{1\text{-loop}}[\mathcal{O}(\alpha)]$, stands for a part of one-loop amplitude not suppressed by Yukawa coupling (m_f^2) contrary to the Born amplitude $\mathcal{A}^{\text{Born}}[\mathcal{O}(m_f^2)]$ and to the rest of one-loop amplitude $\mathcal{A}^{1\text{-loop}}[\mathcal{O}(m_f^2\alpha)]$.

For this reason Born amplitude typically contribute less than the one-loop one and the squared amplitude becomes:

$$|\mathcal{A}^{\text{Born}+1\text{-loop}}|^2 \longrightarrow |\mathcal{A}^{\text{Born}}[\mathcal{O}(m_f^2)] + \mathcal{A}^{1\text{-loop}}[\mathcal{O}(\alpha)]|^2. \quad (3)$$

For the first generation fermions even $\mathcal{A}^{\text{Born}}$ could be neglected, but it can be significant for the second and third generations. The QED one-loop and the bremsstrahlung corrections contribute to the third term of Eq.(2), so they could be also neglected.

Then SANC computes the analytical expressions of the HA for all three channels separately making an appropriate permutation of incoming momenta and projecting CA to the states with definite helicities. Three cross channels of the process $f_1\bar{f}_1HA \rightarrow 0$ and the momenta flow of particles involved are schematically given in Fig. 3.

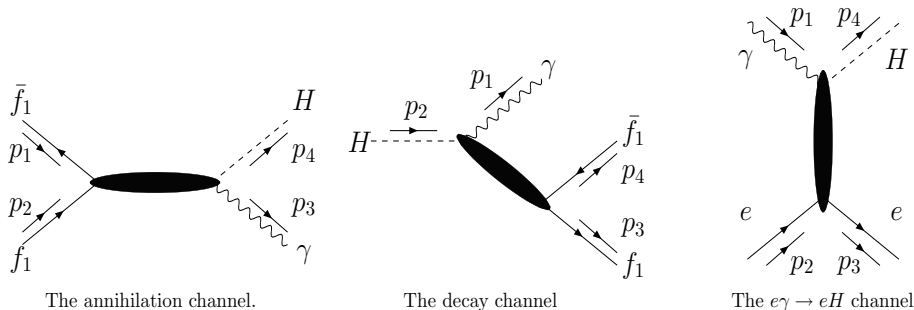


Figure 3: Three and four particle EW processes available in SANC version 1.10

HA for all three channels are presented in Ref. [16]. Here we give only some numerical results for every channel.

3.3.1 Annihilation channel $f_1\bar{f}_1 \rightarrow HA$

The Fig. 4 shows one-loop corrected cross section of the Higgs boson production via annihilation process as a function of the Higgs boson mass, M_H in the same style as Fig. 2 of Ref. [61].

Though we did not manage to perform a “tuned” comparison of our results, there is a good “visual” agreement with Fig. 2 of Ref. [61].

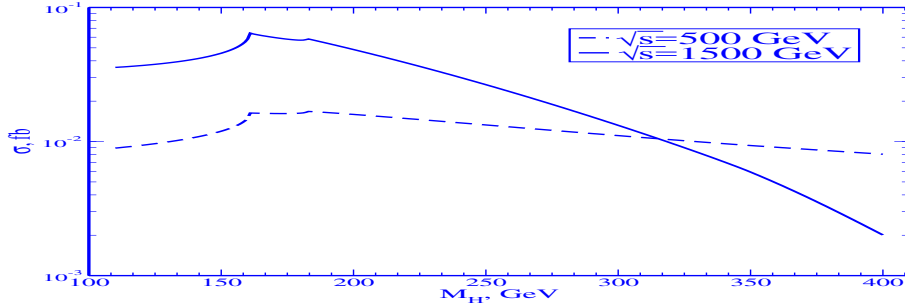


Figure 4: Completely EW corrected σ in fb, as function of the Higgs boson mass

3.3.2 Decay channel $H \rightarrow \mu^+\mu^-\gamma$

For the decay channel we did not find a reference whom to compare with. In the Fig. 5 we show the $M_{\mu^+\mu^-}$ invariant mass distribution at the Born and one-loop levels for $M_H = 150\text{GeV}$.

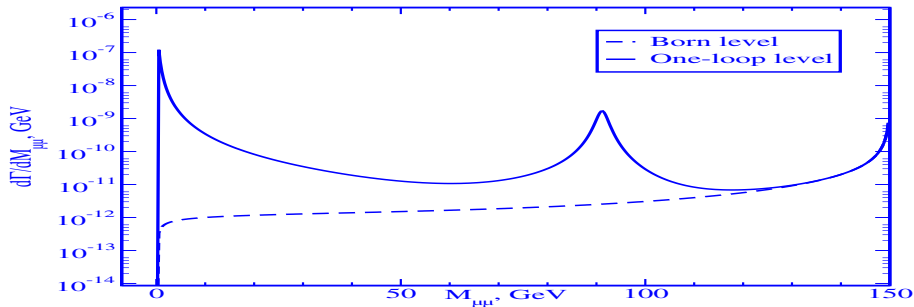


Figure 5: Invariant mass distribution, Born (dashed) and one-loop levels (solid line)

The two peaks due to γ and Z exchanges are distinctly seen. The Born contribution is small everywhere except for the soft photon corner, where it develops an infrared divergence. More numerical results are presented in Ref. [16].

3.3.3 Production channel $e\gamma \rightarrow eH$

For this channel, we present an almost tuned comparison between the results shown in Table I of Ref. [62] and SANC for three cms energies $\sqrt{s} = 500, 1000, 1500$ GeV and wide range of Higgs mass: $110 \text{ GeV} \leq M_H \leq 400 \text{ GeV}$.

In the Table 1 we show total cross sections σ and relative difference δ between the two calculations ($\delta = \sigma[62]/\sigma[\text{SANC}] - 1$, (%)). As seen, the difference in many of points is below 1% and shows up an irregular behavior pointing to its numerical origin (our numbers are calculated with real*16). We consider the two results to be in a very good agreement.

M_H/\sqrt{s}	500			1000			1500		
	SANC	[62]	δ	SANC	[62]	δ	SANC	[62]	δ
80	8.40	8.38	-0.2	9.31	9.29	-0.2	9.76	9.74	-0.2
100	8.85	8.85	0	9.95	9.94	-0.1	10.48	10.5	-0.2
120	9.77	9.80	0.3	11.16	11.2	0.4	11.80	11.8	0
140	11.76	11.8	0.3	13.68	13.7	0.1	14.52	14.6	0.6
160	20.91	21.1	0.9	24.82	25.0	0.7	26.48	26.6	0.5
180	20.67	20.9	1.1	25.04	25.3	1.0	26.81	27.0	0.7
200	16.99	17.2	1.2	21.05	21.2	0.7	22.64	22.8	0.7
300	5.90	5.97	1.2	8.44	8.53	1.0	9.33	9.43	1.1
400	1.64	1.64	0	2.74	2.78	1.5	3.15	3.18	1.0

Table 1: Total cross sections σ in pb and relative difference δ in % between SANC and Ref. [62].

3.4 Three channels of $f_1\bar{f}_1ZA \rightarrow 0$

We implemented three cross channels of $f_1\bar{f}_1ZA \rightarrow 0$: annihilation, $f_1\bar{f}_1 \rightarrow ZA$; decay, $Z \rightarrow f_1\bar{f}_1A$, and production, $e\gamma \rightarrow eZ$, [20].

\sqrt{s} , GeV	θ		DD [63]	Grace-loop [53]	SANC [20]
500	$20^\circ < \theta < 160^\circ$	σ^{Born} , pb	0.7051	0.70515	0.70515
		δ , %	-25.69	-25.689	-25.690
	$1^\circ < \theta < 179^\circ$	σ^{Born} , pb	1.770	1.7696	1.7697
		δ , %	-22.31	-22.313	-22.313
2000	$20^\circ < \theta < 160^\circ$	σ^{Born} , pb	0.04620	0.046201	0.046201
		δ , %	-39.53	-39.529	-39.529
	$1^\circ < \theta < 179^\circ$	σ^{Born} , pb	0.1170	0.1170	0.11697
		δ , %	-30.84	-30.845	-30.845

Table 2: Comparison of the Born cross section pb and δ in % of the $\gamma e^- \rightarrow Ze^-(\gamma)$ reaction ([DD] input and $E_\gamma \leq 0.025\sqrt{s}$ GeV).

For every channel SANC generates the corresponding hard photon emission contribution [20]. We found a paper whom to compare with by A. Denner and S. Dittmaier (DD) [63]. In Table 2 we show only a part of their Table 5.3 where we also added Grace-loop numbers taken from Ref. [53]. As seen, there is perfect agreement between three calculations with the same input.

3.5 Two channels of $\bar{f}_1f_1HZ \rightarrow 0$

The calculations of this process in two channels: annihilation $\bar{f}_1f_1 \rightarrow HZ$ and decay $H \rightarrow Z\bar{f}_1f_1$ are presented in Ref. [12]. Here we present only its CA and several numerical results.

3.5.1 Covariant amplitude of the process

The reason of presenting CA for this process is its compactness, it is described by 6 structures and 6 form factors. Introducing all incoming momenta as $\bar{f}_1(p_1)f_1(p_2)Z(p_3)H(p_4) \rightarrow 0$, one has:

$$\begin{aligned} \mathcal{A}_{ffHZ} &= k \left\{ \left[\bar{v}(p_1) (\gamma_\nu \gamma_+ \sigma_f \mathcal{F}_0^+(s, t) - \not{p}_3 \gamma_+ (p_1)_\nu \mathcal{F}_1^+(s, t) - \not{p}_3 \gamma_+ (p_2)_\nu \mathcal{F}_2^+(s, t)) u(p_2) \varepsilon_\nu^Z(p_3) \right] \right. \\ &+ \left. \left[\sigma_f \rightarrow \delta_f, \gamma_+ \rightarrow \gamma_-, \mathcal{F}_i^+(s, t) \rightarrow \mathcal{F}_i^-(s, t) \right] \right\}, \end{aligned} \quad (4)$$

$$\text{where } \gamma_\pm = 1 \pm \gamma_5, \quad \sigma_f = v_f + a_f, \quad \delta_f = v_f - a_f, \quad k = -\frac{ig^2}{4c_w^2} \frac{M_Z}{M_Z^2 - s}. \quad (5)$$

3.5.2 Annihilation channel $e^+e^- \rightarrow HZ$

For the annihilation channel we present the results of a triple comparison, see Table 3: Again,

\sqrt{s} , GeV	M_H , GeV	Grace-Loop [53]	[64]	SANC [12]
500	100	4.1524	4.1524	4.1524
500	300	6.9017	6.9017	6.9017
1000	100	-2.1656	-2.1656	-2.1656
1000	300	-2.4995	-2.4995	-2.4995
1000	800	26.1094	26.1094	26.1094
2000	100	-11.5413	-11.5414	-11.5414
2000	300	-12.8226	-12.8226	-12.8226
2000	800	11.2468	11.2468	11.2468

Table 3: EW corrections to the total cross section in percent in α scheme.

one observes an excellent agreement between three calculations. In **SANC** we implemented also complete NLO EW corrections, including hard photon bremsstrahlung.

3.5.3 Decay channel $H \rightarrow Z f_1 \bar{f}_1(\gamma)$

For the decay channel we did not find a paper whom to compare with. In Fig. 6 we show distributions over invariant mass $m_{\mu^+\mu^-(\gamma)}^2$. A narrow peak at low mass is distinctly seen. It has simple physical explanation. Since the $H \rightarrow Z\gamma$ width does not vanish for an on-shell photon with $Q_\gamma^2 = 0$, the one-loop amplitude for $H \rightarrow Z f_1 \bar{f}_1$ with virtual photon exchange will show a $\sim 1/s$ behavior (with $s = -Q_\gamma^2$). This, in turn, will lead to the $\sim 1/s$ behavior of both the double and single differential widths. The $1/s$ region is very narrow and is largely washed out not only by a soft cut on the variable s but even by the plain s -integration.

3.5.4 $H \rightarrow Z f_1 \bar{f}_1$: a MC generator for $H \rightarrow 4\mu$ decay

Based on results of previous section, we developed a simple MC event generator which takes into account: identity of muons, one photon radiation and one-loop EW virtual corrections in the resonance approximation. The idea of this approach is described in more details in

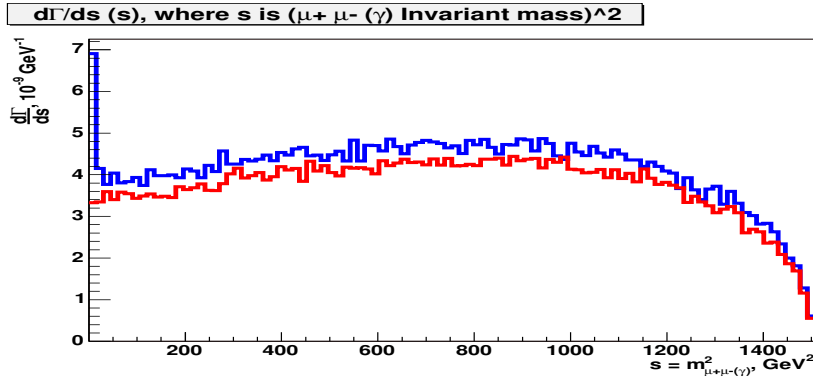


Figure 6: The distributions over invariant mass $m_{\mu^+\mu^-(\gamma)}^2$ in α scheme. The red line shows Born level distribution while blue line — Born+1loop.

Ref. [12]. As was shown in [12], this approximation is valid for $130 \leq M_H \leq 160$ GeV. This event generator was transferred for use to JINR ATLAS muon group.

3.5.5 MC $H \rightarrow 4\mu$: Prophecy4f & SANC comparison

Recently there appeared a MC generator Prophecy4f based on a complete 5-point one-loop calculations Refs. [36, 65, 66]. We present a Table of comparison for partial width for decay $H \rightarrow 4\mu$ in G_μ scheme for $M_H = 140$ GeV between Prophecy4f and SANC.

M_H , GeV	120	130	140	150	160
Prophecy4f	0.7053(3)	2.3769(9)	6.692(2)	16.807(6)	40.06(1)
SANC (G_μ)	0.7197(3)	2.4079(8)	6.743(2)	16.842(5)	39.62(2)
δ , %	2.04	1.01	0.76	0.21	-1.10
SANC (α)	0.6938(2)	2.343(1)	6.594(2)	16.534(5)	39.15(1)

Table 4: Comparison for partial width in 10^{-7} GeV for decay $H \rightarrow 4\mu$ in G_μ scheme for $M_H = 140$ GeV between Prophecy4f and SANC

As seen from the Table 3.5.5, there is $\pm 1\%$ agreement in the mass range 130–140 GeV, degrading at the edges of the interval [120–160] as expected, see Ref. [12]. Note, that Prophecy4f uses another renormalization scheme and takes into account several higher order effects and that SANC calculations in α and G_μ schemes differ by about 2%.

The SANC generator was used for a MC simulation of $H \rightarrow 4\mu$ decay in the ATLAS detector and the results were compared with those obtained by PYTHIA, showing notable deviations.

3.6 Drell–Yan-like W and Z production

The description of Drell–Yan-like single W and Z production processes are rather advanced in SANC. As usual, we begin with partonic level calculations by running relevant FF/HA/BR

files each by FORM and s2n.

3.6.1 CC and NC Drell–Yan processes distributions

The FORTRAN modules, generated by `s2n` package, are used in MC integrators and generators based on Vegas algorithm. With the aid of the integrators we have produced numerous distributions presented in proceeding of Les Houches [36] and TeV4LHC [37] Workshops. Here we present a few distributions, both for CC and NC cases. The results obtained with the aid of generators will be presented elsewhere.

First of all, one has to introduce some notions.

- Charged current Drell–Yan (CC DY) production:
 - $q\bar{q}'$ sub-process, $p[q] + p[\bar{q}'] \rightarrow W^\pm \rightarrow X + \ell^\pm + \nu_\ell(+\gamma)$
 - gq sub-process, $p[g] + p[q] \rightarrow W^\pm \rightarrow X + \ell^\pm + \nu_\ell(+g)$
 - γq or γ -induced sub-process
 $p[\gamma] + p[q] \rightarrow W^\pm \rightarrow X + \ell^\pm + \nu_\ell(+\gamma)$, ($\ell = e, \mu$)
- Neutral current Drell–Yan (NC DY) production:
 - $q\bar{q}$ sub-process, $p[q] + p[\bar{q}] \rightarrow \gamma, Z \rightarrow X + \ell^+ + \ell^- (+\gamma)$
 - gq sub-process, $p[g] + p[q] \rightarrow \gamma, Z \rightarrow X + \ell^+ + \ell^- (+g)$
 - γq or γ -induced sub-process
 $p[\gamma] + p[q] \rightarrow \gamma, Z \rightarrow X + \ell^+ + \ell^- (+\gamma)$, ($\ell = e, \mu$)

For CC we computed $2 \otimes 2 \otimes 2$ distributions:

$$\begin{pmatrix} q\bar{q}' \\ g(\gamma)q \end{pmatrix} \otimes \begin{pmatrix} p_T \\ M_T \end{pmatrix} \otimes \begin{pmatrix} \mu \\ e \end{pmatrix}$$

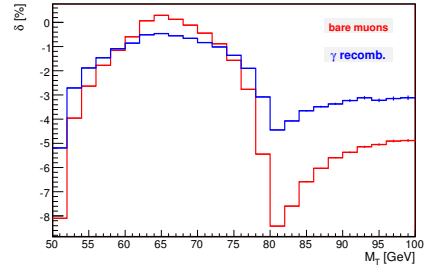
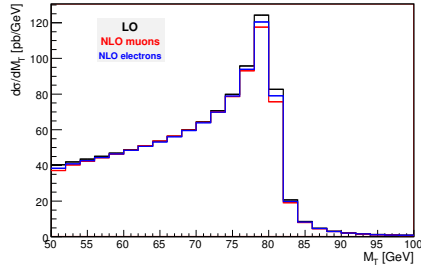
In the first column the partons participating a hard sub-process are shown. In the second column — the variable of distribution: transverse leptonic momentum $p_T = p_T^\ell$ or transverse mass $M_T = \sqrt{2p_T^\ell p_T^\nu (1 - \cos \varphi_{\ell\nu})}$ of $\ell\nu_\ell$ system. In the third column — the type of final charge lepton μ or e . Moreover, for muons we use the so-called “bare” setup and for electrons — “calo” set up with some $e-\gamma$ recombination, see above mentioned Proceedings.

For NC case only middle column has different and obvious meaning.

$$\begin{pmatrix} q\bar{q} \\ g(\gamma)q \end{pmatrix} \otimes \begin{pmatrix} p_T \\ M_{\ell^+\ell^-} \end{pmatrix} \otimes \begin{pmatrix} \mu \\ e \end{pmatrix}$$

For initial parton = γ we finished a recent paper [27]. We have also distributions with initial parton = *gluon*, but they are still preliminary and we will not show them in this report.

The distributions are produced for the cross-sections σ (pb) and the relative corrections δ (%) where the last is defined by $\delta = \sigma^{1\text{-loop}}/\sigma^{\text{Born}} - 1$ for NLO QCD and EW corrections originating from the $q\bar{q}'$ sub-process and by $\delta = \sigma^{g(\gamma)q}/\sigma^{\text{Born}}$ for corrections originating from

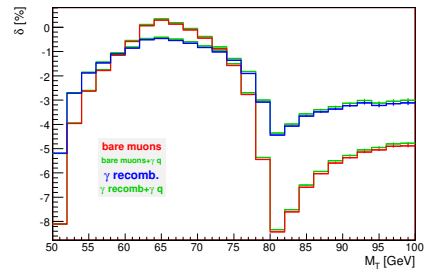
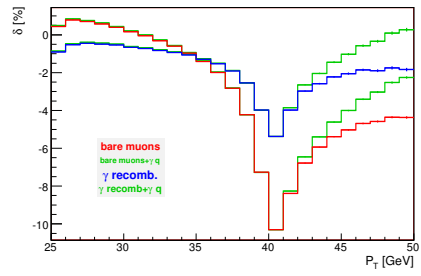


the gluon (photon) induced processes.

CC DY: σ and δ , M_T distribution The EW correction is lower for the electrons due to recombination with photons.

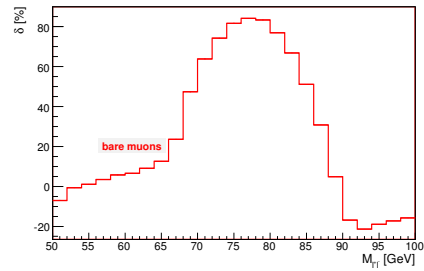
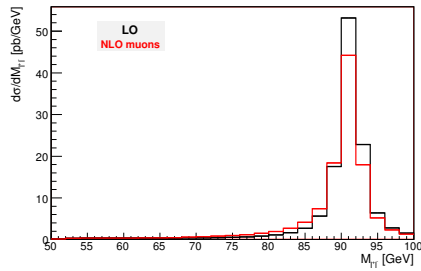
The following two figures illustrate the contribution of γ -induced processes.

CC DY: δ , P_T^ℓ and M_T distribution



As seen, they are quite prominent in P_T^ℓ distribution and barely visible in M_T distribution.

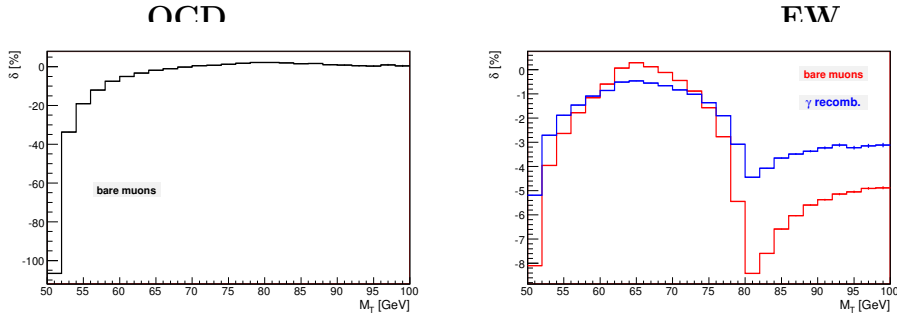
NC DY: σ and δ , $M_{\ell+\ell^-}$ distribution



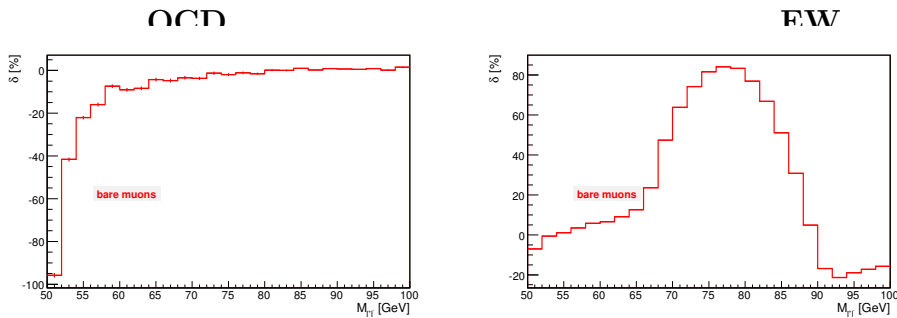
3.6.2 QCD-EW interplay

One of the most interesting questions in connection with Drell–Yan processes is the interplay of EW and QCD corrections at least in the NLO approximation. With the aid of SANC it is possible since we implemented NLO QCD correction exactly in the same language as we did for EW ones.

CC DY: δ , M_T distribution



NC DY: δ , $M_{\ell^+\ell^-}$ distribution



From these figures one may conclude that at least for some distributions NLO QCD corrections do not dominate. A more detailed presentation of this issue may be found in our reports to ATLAS MC working group.

An example of tuned triple comparison within TEV4LHC workshop [37]

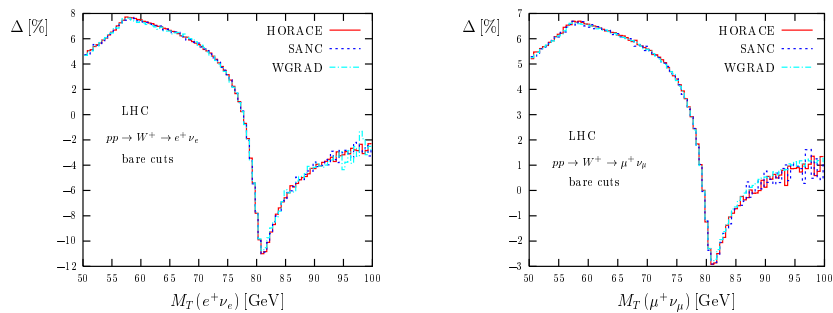


Figure 7: The relative correction Δ due to electroweak $\mathcal{O}(\alpha)$ corrections to the M_T distribution for single W^+ production with bare cuts at the LHC.

This figure illustrates that the issue of “technical precision” of EW NLO corrections for CC DY is well under control.

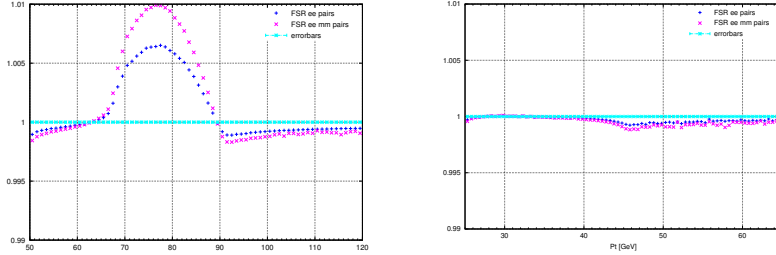


Figure 8: Relative light pair corrections to invariant mass (left) and transverse momentum (right) distribution in $\mu^+\mu^-$ production.

3.6.3 Light pair corrections to Drell-Yan processes

Light pair emission from the final state is analogous to the effect of the final state radiation (FSR) of photons. The latter was scrutinized in [28],[29]. It was shown that the photonic FSR for some observables provide corrections of the order of several dozens of percent. Light pair radiation is suppressed with respect to the photonic one by the additional factor α , but taking it into account is obviously important. The bulk of the effect is coming from e^+e^- pair emission. The contribution of $\mu^+\mu^-$ pairs is estimated as well. As an illustration we present Figure 8 where relative pair corrections are presented to the differential distributions in the (primary) muon pair invariant mass and the muon transverse momentum in the process $p + p \rightarrow Z + X \rightarrow \mu^+ + \mu^- + X$. These results were produced by means of the SANC Monte Carlo integrator. They were submitted to the W-mass workshop proceedings and compared with the results of analogous calculations by the HORACE computer code.

3.7 4-boson study: $\gamma\gamma \rightarrow \gamma\gamma$, $\gamma\gamma \rightarrow \gamma Z$, $Z \rightarrow \gamma\gamma\gamma$, $\gamma\gamma \rightarrow ZZ$

The estimation of four-bosons background processes is very important for new physics searches. For example, according to SM calculations for $\gamma\gamma \rightarrow \gamma Z$ process the number of background events is about 5×10^3 to 3×10^4 corresponding to clear $\gamma\gamma \rightarrow H \rightarrow \gamma\gamma$ signal of about 45 to 70 events per 500 fb^{-1} luminosity for the 160 to 320 GeV energy range on $\gamma\gamma$ -mode of a linear e^+e^- -machine. To study Higgs boson properties one needs to have angular distributions for each helicity amplitude of these processes

The evaluations for processes (6), (7), (8) were presented in [24], [25] and [26]

$$\gamma\gamma \rightarrow \gamma\gamma, \tag{6}$$

$$Z \rightarrow \gamma\gamma\gamma, Z\gamma \rightarrow \gamma\gamma, \tag{7}$$

and

$$\gamma\gamma \rightarrow ZZ, \tag{8}$$

in the Standard Model (SM) at the one-loop level of accuracy in R_ξ -gauge through fermion loops and corresponding precomputation blocks. with taking into account of all masses (Z boson and internal ones). The computations of these processes take into account non-zero masses of loop-fermions. The additional precomputation modules used for calculation of massive fermion-box diagrams briefly described. In these papers we discussed the covariant

and tensor structures for these processes and present them in a compact form. The helicity amplitude approach and their expressions are given. The corresponding packages for numeric calculations are available on request. More details are presented in our first publications about the four boson sector in [24].

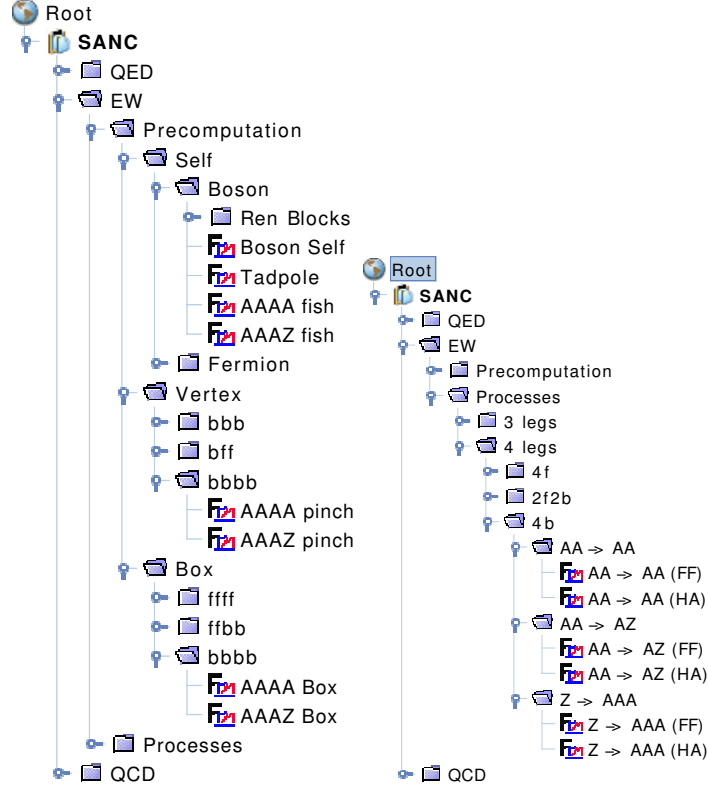


Figure 9: $Z\gamma\gamma\gamma \rightarrow 0$ extension of SANC processes tree.

Let us demonstrate the CA for these three processes.

The full CA of the process (6) for off-shell photons ($p_i\epsilon_i \neq 0$) can be written as:

$$\mathcal{A}_{\gamma\gamma\rightarrow\gamma\gamma} = 4e^4Q_f^4 \sum_{i=1}^{43} \mathcal{F}_i(s, t, u) T_i^{\alpha\beta\mu\nu}, \quad (9)$$

where e is the electron charge, Q_f is the charge of the loop fermion in units of e , $T_i^{\alpha\beta\mu\nu}$ are tensors defined with the aid of auxiliary strings τ_j ; \mathcal{F}_i are FFs that depend on invariants s, t, u and also on fermion masses and Passarino–Veltman functions. The off-shell process contains 43 basis elements.

In terms of Lorentz structures the expression for the CA $Z\gamma\gamma\gamma \rightarrow 0$ is:

$$\mathcal{A}_{Z\gamma\gamma\gamma\rightarrow 0} = 4e^4Q_f^4 \sum_{i=1}^{14} \left[\mathcal{F}_i^{\text{bos}}(s, t, u) + \mathcal{F}_i^{\text{fer}}(s, t, u) \right] T_i^{\alpha\beta\mu\nu}. \quad (10)$$

and in the same spirit the CA $ZZ\gamma\gamma \rightarrow 0$ is

$$\mathcal{A}_{\gamma\gamma\rightarrow ZZ} = 4e^4 Q_f^4 \sum_{i=1}^{20} [\mathcal{F}_i^{\text{bos}}(s, t, u) + \mathcal{F}_i^{\text{fer}}(s, t, u)] T_i^{\alpha\beta\mu\nu}. \quad (11)$$

3.8 Auxiliary J functions

In papers [57], [58] we begin to study a special class of Passarino-Veltman functions J arising at the reduction of infrared divergent box diagrams. The work presented in [59] continues the study of infrared and mass singularities emerging from 4-point function box diagrams with an internal photon line connecting two external lines on the mass shell, for example of the process $ud \rightarrow WA$. This is an extension of earlier investigations of the calculation of diagrams of such class.

By construction, J functions are free of infrared singularities and are made sufficiently simple for subsequent integration over the three Feynman parameters z, x, y , leading to a compact explicit result in terms of dilogarithm functions.

$$i\pi^2 J = \mu^{4-n} \int d^n q \frac{v(q, p_i) \cdot v(p_i)}{d_0 d_1 d_2 d_3}. \quad (12)$$

The function J , in turn, may be subjected to the standard Passarino-Veltman reduction giving linear combinations of the standard D_0 and C_0 functions, which may be used to exclude complicated infrared divergent D_0 function in favour of J function and simplest 3-point infrared divergent C_0 function.

In general, the explicit form of J function is not universal, depending on the concrete topology of the infrared divergent D_0 function of a process.

There was found a way to introduce a universal function by means of a special trick to simplify the analytic calculations, choosing two 4-vectors and Feynman parametrisation in the defining expression for functions J , Eq. (12), which ensures linear dependence of the integrand of J on one of the integration variables, x , Eq. (13).

$$J = \int_0^1 dx \int_0^1 y dy N_{xy} \int_0^1 dz \frac{z}{(L - zk_{xy}^2)^2}. \quad (13)$$

In this way, one obtains the expression for J in terms of the universal auxiliary function $J_{\text{uni}}(P_1^2, P_2^2; m_1, m_2, m_3, m_4)$. This allows to obtain explicit expression for various topologies by a simple rotation of its dummy arguments. This approach leads to compact analytical results, allows one to perform stable and fast numerical calculations and avoid large numerical cancellations between separate terms. A detailed comparison of numerical results with the Loop Tools package showed agreement at a very good level.

4 SANC, application to ATLAS

SANC, application to ATLAS physics: increasing of the theoretical precision of the predictions: • evaluation of the so-called “missed higher order corrections”, that is those which are not taken to the account by the standard ATLAS programs for simulation of the cross sections of the W and Z bosons production [67], [68]; • creation of advanced versions of Monte-Carlo tools (integrator and generator) for the analysis of LHC data taking into account the interplay of next-to-leading (NLO) QCD and EW corrections. mcsanc integrator for the first time realizing within a unified approach precision Monte-Carlo simulation for a series of processes representing an interest for LHC physics at the NLO level. These tools appended by a calculation of NNLO QCD contributions with an aid of programs by other groups, were already used in the analysis of LHC data, see [33]; • analysis of the contribution of QED radiation from final state charged leptons for the processes at LHC was performed [30] and [28] • participation in International CERN Workshop between top codes: POWHEG, FEWZ, DYNNLO, HORACE, WZGRAD2, RADY, SANC, PHOTOS. “Benchmarks for Drell-Yan processes at the LHC”. [38]

4.1 MCSANC integrator

The list of processes implemented in the MCSANC integrator includes Drell-Yan processes (inclusive), associated Higgs and gauge boson production and single-top quark production in s- and t-channel (see Figure 4.1) [30]. The MCSANC integrator is suited for simulation of realistic distributions of these processes taking into account LHC experimental conditions. The code allows to study how various radiative corrections affect the distributions.

The scheme of the SANC framework is shown on the Figure 10. Analytical expressions are obtained for the formfactors and amplitudes of generalized processes $f\bar{f}b\bar{b} \rightarrow 0$ and $4f \rightarrow 0$ and stored as the FORM language expressions. The latter are translated to the Fortran modules for specific parton level processes with NLO QCD and EW corrections. The modules are utilising LoopTools and SANCLib packages for loop integrals evaluation. To build a Monte Carlo code one convolutes the partonic cross sections from the modules with the parton density functions and feeds the result as an integrand to any Monte Carlo algorithm implementation, e.g. FOAM or Cuba. The module’s procedures for partonic cross sections are significantly unified and allow to calculate fully differential hadronic cross sections.

Below we provide numerical cross checks for the MCSANC integrator. The SANC DY NLO electroweak corrections were thoroughly compared with other calculations earlier during theoretical workshops on the subject. The newer QCD results are validated using the MCFM program.

Table 5 contains results for integrated LO and NLO EW and QCD cross sections obtained

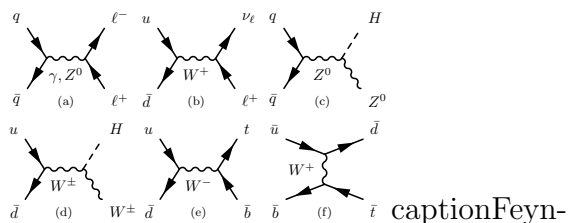


Figure 4.1: Feynman graphs for tree level Drell-Yan process neutral (a) and charged (b) currents, Higgs and gauge boson production neutral (c) and charged (d) currents, and single top-quark production s-channel (e) and t-channel (f) implemented in the MCSANC integrator.

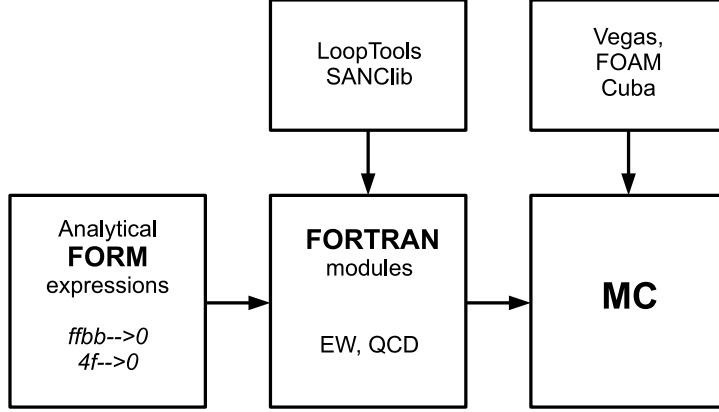


Figure 10: The SANC framework scheme.

$pp \rightarrow$	$Z^0(\mu^+\mu^-)$	$W^+(\mu^+\nu_\mu)$	$W^-(\mu^-\bar{\nu}_\mu)$
LO	3338(1)	10696(1)	7981(1)
LO MCFM	3338(1)	10696(1)	7981(1)
NLO QCD	3388(2)	12263(4)	9045(4)
NLO MCFM	3382(1)	12260(1)	9041(5)
NLO EW	3345(1)	10564(1)	7861(1)
$\delta_{QCD}, \%$	1.49(3)	14.66(1)	13.35(3)
$\delta_{EW}, \%$	0.22(1)	-1.23(1)	-1.49(1)

Table 5: NC and CC DY processes. LO, NLO EW, NLO QCD cross sections are given in picobarns and compared with corresponding values obtained with the program MCFM. The correction factors δ are shown in %.

with the MCSANC integrator. The LO and NLO QCD values are in agreement with the MCFM program within statistical errors. A detailed comparison of differential neutral current Drell-Yan cross section is shown on Figure 11 for dilepton invariant mass distribution. The right plot shows a good agreement between NLO QCD correction factors obtained with MCSANC and MCFM.

In the MCSANC-v1.20 version of the Monte-Carlo tool based on the SANC modules, the inverse photon - ($q\gamma$) and ($\gamma\gamma$) configurations in the initial pp state of beam - contributions to the Drell-Yan processes are added.

The MCSANC-v1.20 version was used to calculate the following corrections to the Drell-Yan processes at $\sqrt{s} = 13$ TeV:

- the missed - pure weak, initial and interference QED - one-loop contributions to the M_{inv} distribution;
- the inverse photons contributions for fiducial cuts.

The predictions were calculated in the following fiducial volumes:

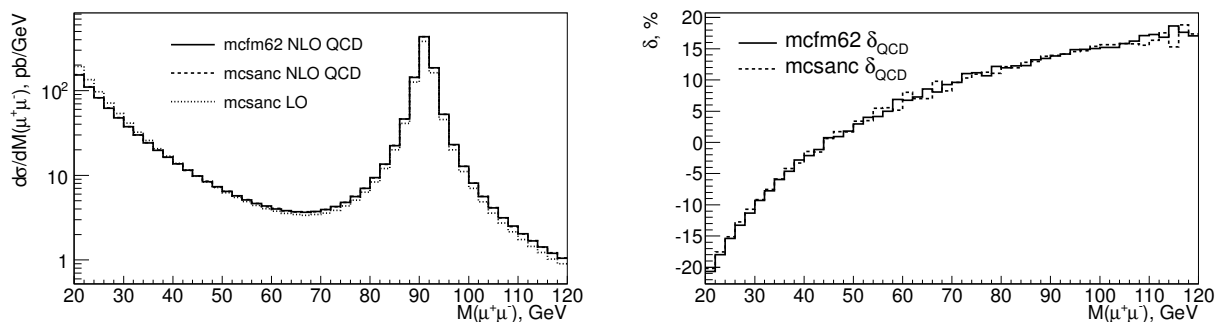


Figure 11: Comparison of differential cross sections and correction factors $\delta(\text{QCD})$ for neutral current Drell–Yan $pp \rightarrow \mu^+\mu^-$ process in dimuon invariant mass distribution.

- neutral current: $p_T(\ell) > 30\text{GeV}$ and $|\eta(\mu)| < 2.4$ or $|\eta(e)| < 2.47$ for muon or electron channel, respectively;
- charged current: $M_T > 60\text{GeV}$, $p_T(\mu) > 30\text{GeV}$, $E_T(\nu_\mu) > 30\text{GeV}$ and $|\eta(\mu)| < 2.4$ for muon channel, and $M_T > 60\text{GeV}$, $p_T(e) > 65\text{GeV}$, $E_T(\nu_e) > 65\text{GeV}$ and $|\eta(e)| < 2.47$ for electrons

The obtained results were used by the ATLAS Standard Model group for Drell-Yan data analysis.

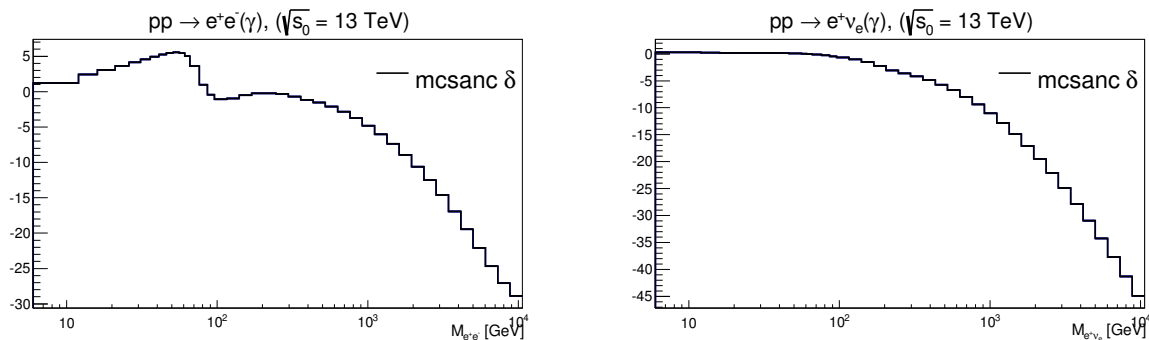


Figure 12: δ_{MISS} contribution $pp \rightarrow e+e-(\gamma)$ (left) and $pp \rightarrow e^+\nu_e(\gamma)$ right at $\sqrt{s} = 13\text{TeV}$.

With paper [31] we continue the series of works dedicated to the development of MCSANC, a Monte Carlo tool based on the SANC modules. We present an update of the integrator up to v.1.20 with inclusion of the aforesaid corrections relevant for DY processes at the LHC at $\sqrt{s} = 13\text{TeV}$. We briefly review the implementation into the framework of the MCSANC v.1.20 tool the following three new options: • photon-induced contributions. The implemented processes are: $q\gamma \rightarrow ql^\pm\nu_l$ (for CC DY), $q\gamma \rightarrow ql^+l^-$ (for NC DY) and $\gamma\gamma \rightarrow l^+l^-$ (for NC DY); • leading in Gm_t^2 two-loop EW and mixed EW \otimes QCD radiative corrections; • forward-backward asymmetry A_{FB}^{ff} .

Recent activities was overview in [32] “Computer system SANC: its development and applications”,

4.2 Electroweak corrections for ATLAS Drell–Yan analysis

Monte Carlo simulations in ATLAS analysis are typically based on the NLO QCD hard process event generators like POWHEG++ or MC@NLO complemented with PHOTOS to generate final state electromagnetic radiation. This approach does not take into account a set of higher order electroweak corrections (HO EW) when considering Drell–Yan processes: pure weak (PW) contributions, initial–final QED interference (IFI) and what remains from initial state radiation (ISR) after subtraction of collinear divergences. These corrections are sometimes referred in this text under term “missed”.

Importance of these corrections in the DY analysis have been demonstrated in the ATLAS internal note ATL-PHYS-INT-2011-081 and [33]. Figure 13 shows distribution of $d\delta/dM_{\ell\ell} = (d\sigma^{\text{Born+NLO}}/dM_{\ell\ell})/(d\sigma^{\text{Born}}/dM_{\ell\ell}) - 1$ in the Z -resonance region. While this correction can be negligible in near the resonance, it becomes more noticeable for outer invariant mass values. This is especially relevant for searches of the heavy dilepton resonances Z' at the LHC.

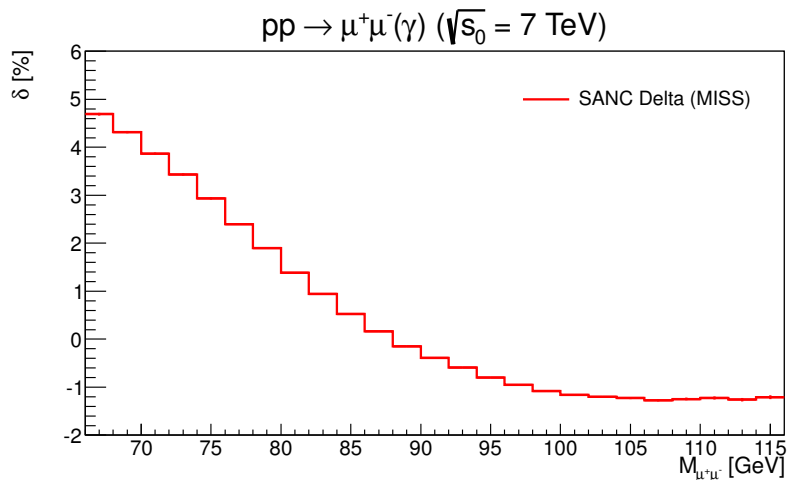


Figure 13: Missed correction δ^{MISS} in % for the distribution over $M_{\mu^+\mu^-}$ around Z resonance.

At present the best fixed order approximation of the Drell–Yan cross section is the NNLO QCD and NLO EW. However, their proper combination requires also calculation of $\mathcal{O}(\alpha\alpha_S)$ contribution, which is currently not available in complete form. In view of it’s importance for the data analysis, two methods of combination of HO EW and QCD corrections in the theoretical predictions were compared in [69]:

- Factorised approach, in which it is assumed that the HO EW corrections are the same for all orders of QCD and thus can be determined at LO QCD in terms of K -factors and then transferred to any higher order of QCD

$$\begin{aligned}
 K_{EW} &= \frac{\sigma_{NLO_{EW}}}{\sigma_{LO}}, \\
 \sigma_{NNLO_{QCD}, NLO_{EW}} &= K_{EW} \times \sigma_{NNLO_{QCD}}.
 \end{aligned}
 \tag{14}$$

- Additive approach assumes that HO EW corrections (except QED FSR) are largely additive and the same term needs to be added to all orders of QCD

$$\begin{aligned}\sigma_{NNLO_{QCD},NLO_{EW}} &= \sigma_{NNLO_{QCD}} + \Delta\sigma_{NLO_{EW}}, \\ \Delta\sigma_{NLO_{EW}} &= \sigma_{NLO_{EW}} - \sigma_{LO}.\end{aligned}\tag{15}$$

This approach is implemented in FEWZ 3.1.b2.

For this comparison the electroweak corrections implemented in FEWZ were thoroughly cross checked with MCSANC code in electroweak G_μ scheme and found to be consistent over wide dilepton invariant mass range and gauge boson rapidity Figure 14.

The comparison of these methods is represented on Figure 15. The overall conclusion of this study is that provided additive method is available (for NC DY processes it's implemented in the FEWZ code), one should chose it for theoretical predictions. In other cases one can use additive approach (DY CC) and use factorised approach to estimate systematic uncertainty. One should note in this case, that consistent result will be only in case all cross sections and K -factors were calculated with the same PDF set of the order of desired final approximation. That means, for σ_{NNLO} one should use NNLO PDF for all calculations, including σ_{LO} .

LHC data provide access to invariant mass regions where photon induced contribution to the Drell–Yan process becomes substantial relative to the quark-antiquark annihilation. More accurate estimation of this background for high mass resonance searches requires inclusion of $\gamma\gamma \rightarrow \ell^+\ell^-$ into the theory predictions. The predictions were obtained using implementation of this process in the MCSANC integrator with MRST2004QED PDF, which albeit deprecated, was the only set containing photon density at that time. The results of this estimation are presented on the Figure 16 together with HO EW except QED FSR corrections, which appear to have opposite sign. The corrections were included as a systematic uncertainty in the ATLAS searches for high mass dilepton resonances [70].

Overall the calculations of HO EW except QED FSR corrections and their NNLO QCD combination methodology were routinely used in the ATLAS Standard Model and BSM analysis:

- Measurements of the Drell–Yan differential cross sections at $\sqrt{s} = 7$ TeV in the e and μ channels for invariant masses between 26 GeV and 66 GeV using an integrated luminosity of 1.6 fb^{-1} collected in 2011 [35]. Theory comparisons show that fixed order next-to-next-to-leading-order QCD predictions provide a significantly better description of the results than next-to-leading-order QCD calculations, see Figure 17.
- Measurements of the high-mass Drell–Yan differential cross sections at $\sqrt{s} = 7$ TeV in the e+e- channel based on integrated luminosity of 4.9 fb^{-1} . Invariant mass of the electrons pair, covered by the measurement is, $116 < M_{ee} < 1500$ GeV [34].
- Measurement of the inclusive W^\pm and Z/γ cross sections in the electron and muon decay channels in pp collisions at $\sqrt{s} = 7 \text{ TeV}$ [67]
- A QCD analysis performed on the ATLAS data of inclusive W and Z boson production, jointly with ep deep inelastic scattering data from HERA. The ATLAS data exhibited

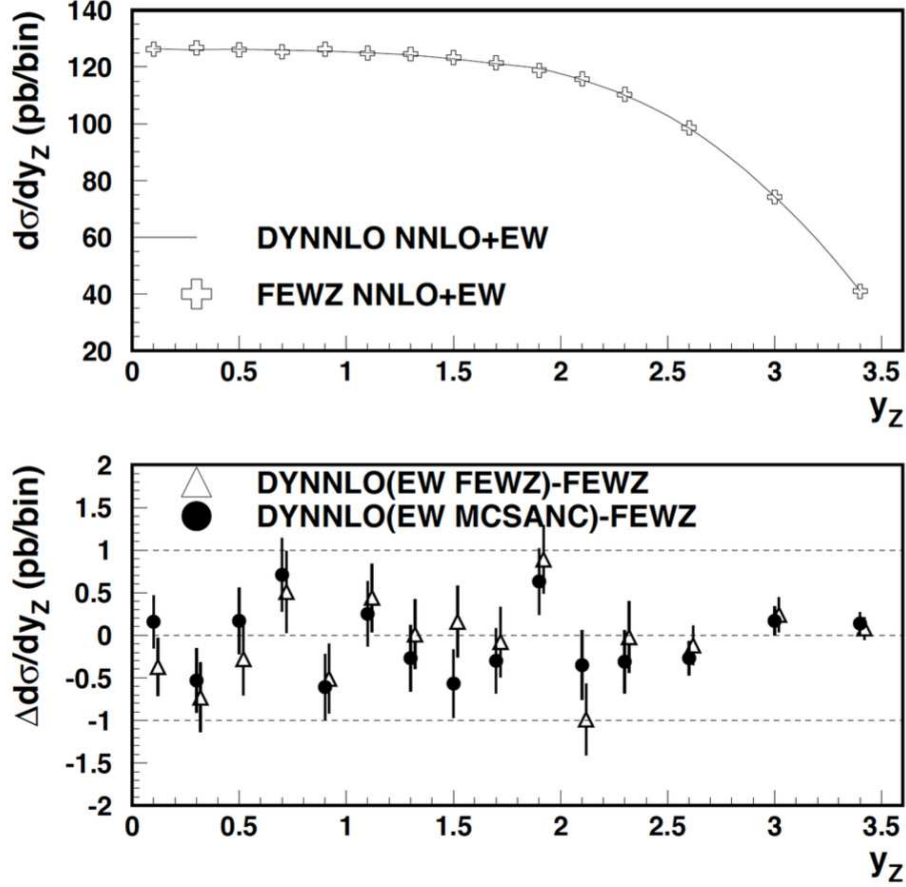


Figure 14: Top: high precision NC DY y_Z predictions using either missing EW (FEWZ) or missing EW (MCSANC) applied in additive way to the NNLO QCD DYNNLO prediction. Bottom: ratio of the predictions.

sensitivity to the light quark sea composition and magnitude at Bjorken $x \sim 0.01$. Specifically, the data supported the hypothesis of a symmetric composition of the light quark sea at low x . The ratio of the strange-to-down sea quark distributions is determined to be $1.00(+0.25-0.28)$ at absolute four-momentum transfer squared $Q^2 = 1.9 \text{ GeV}^2$ and $x = 0.023$ [68]

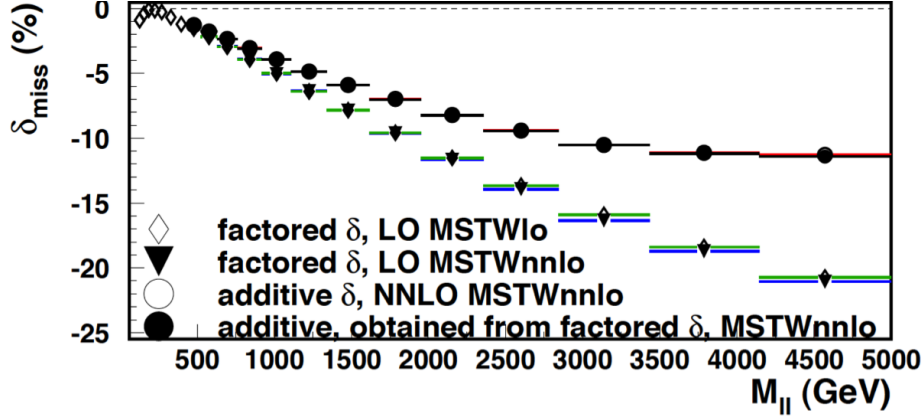


Figure 15: HO EW except QED FSR (δ_{miss} in %) corrections for NC Drell Yan production. Calculations are based on FEWZ 3.1.b2 and $\sqrt{s} = 8$ TeV.

- Search for high-mass dilepton resonances in 20 fb^{-1} of pp collisions at $\text{sqrt}(s) = 8$ TeV. Results are presented from an analysis of proton-proton (pp) collisions at a center-of-mass energy of 8 TeV corresponding to an integrated luminosity of 20.3 fb^{-1} in the dielectron channel and 20.5 fb^{-1} in the dimuon channel. A narrow resonance with Standard Model Z couplings to fermions is excluded at 95% confidence level for masses less than 2.79 TeV in the dielectron channel, 2.53 TeV in the dimuon channel, and 2.90 TeV in the two channels combined. [70]

4.3 Drell–Yan processes: tuned comparison

The tuned comparison of EW corrections for CC Drell–Yan processes was started within the Les Houches Workshop [36], however, much more detailed study was performed within the TEV4LHC Workshop [37]. Three teams participated within TEV4LHC Workshop: • HORACE — C.C. Calame, G. Montagna, O. Nicosini, A. Vicini (Pavia, Italy) [44]–[45]; • SANC — SANC group (JINR, Dubna, Russia) [11]–[13]; • $w(Z)$ GRAD2 — U. Baur, D. Wackerroth (FNAL, USA) [46]–[49]. The report [38] was prepared in the context of the LPCC Electroweak Precision Measurements at the LHC WG and summarizes the activity of a subgroup dedicated to the systematic comparison of public Monte Carlo codes, which describe the Drell–Yan processes at hadron colliders, in particular at the CERN Large Hadron Collider (LHC). This work represents an important step towards the definition of an accurate simulation framework necessary for very high-precision measurements of electroweak (EW) observables such as the W boson mass and the weak mixing angle. All the codes considered in this report share at least next-to-leading-order (NLO) accuracy in the prediction of the total cross sections in an expansion either in the strong or in the EW coupling constant. The NLO fixed-order predictions have been scrutinized at the technical level, using exactly the same inputs, setup and perturbative accuracy, in order to quantify the level of agreement of different implementations of the same calculation. Several examples of higher-order effects due to the strong or the EW interaction are discussed in this common framework. Also the combination

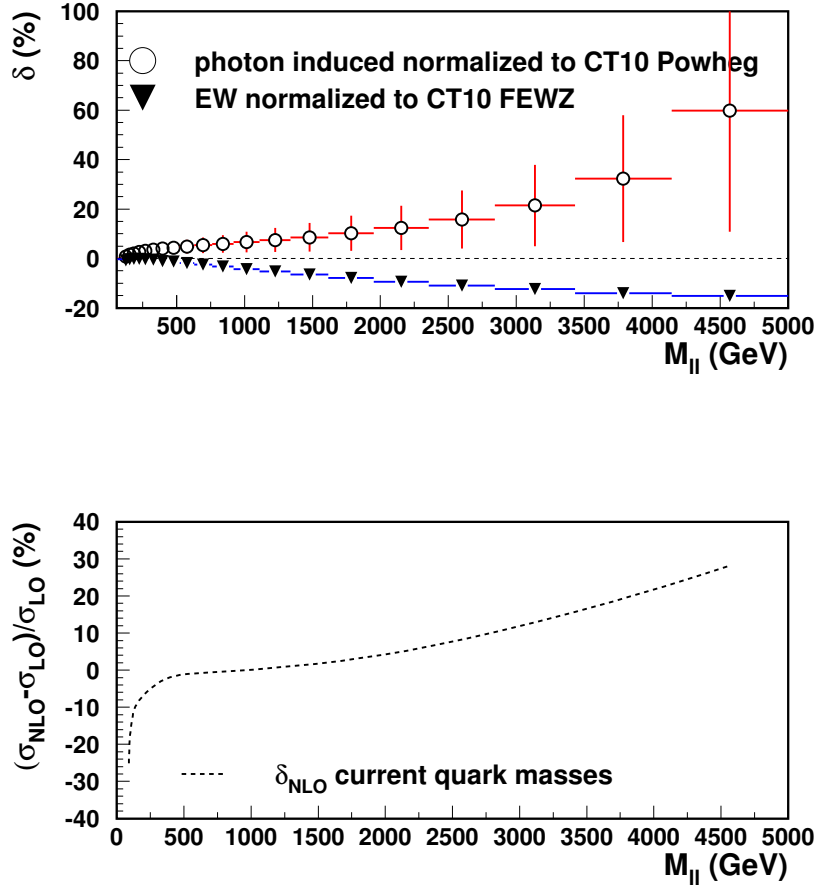


Figure 16: Photon induced background contributions calculated with $p_{T,\ell} > 25$ GeV and $\eta_\ell < 2.5$, MRST2004QED photon PDF and $\sqrt{s} = 8$ TeV over a wide invariant mass range. Calculations are performed with MCSANC [30].

of QCD and EW corrections is discussed, together with the ambiguities that affect the final result, due to the choice of a specific combination recipe. All the codes considered in this report have been run by the respective authors, and the results presented here constitute a benchmark that should be always checked/reproduced before any high-precision analysis is conducted based on these codes. In order to simplify these benchmarking procedures, the codes used in this report, together with the relevant input files and running instructions, can be found in a repository at <https://twiki.cern.ch/twiki/bin/view/Main/DrellYanComparison>.

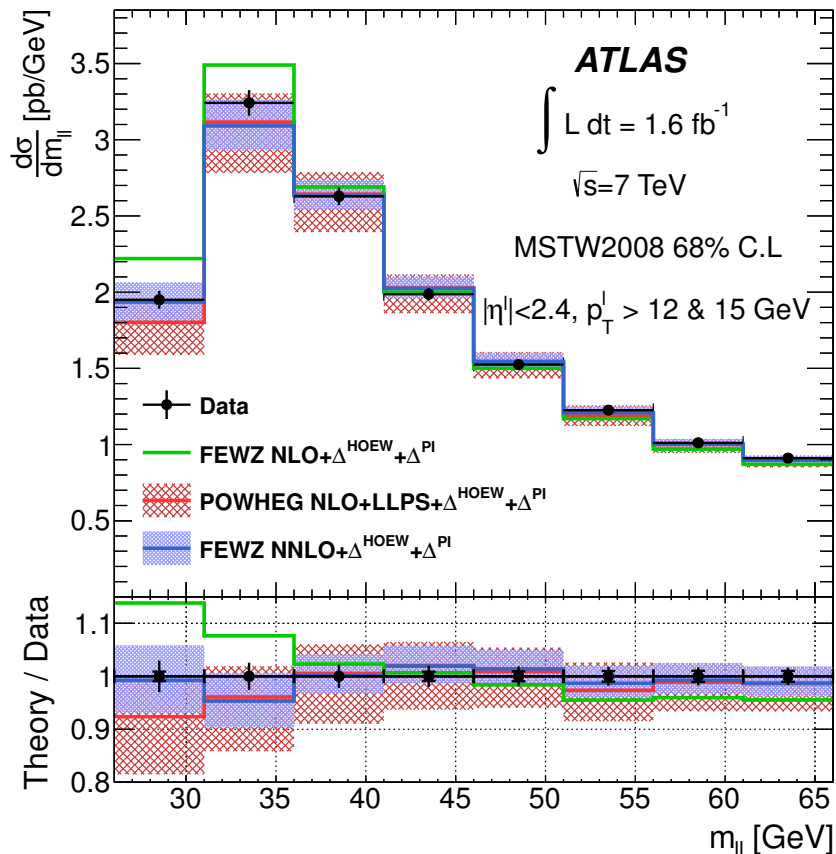


Figure 17: The measured fiducial differential cross section, $\frac{d\sigma}{dm_{\ell\ell}}$ for the nominal analysis as a function of the invariant mass $m_{\ell\ell}$ (solid points) compared to NLO predictions from FEWZ, NLO+LLPS predictions from POWHEG and NNLO predictions from FEWZ (all including higher-order electroweak and photon induced corrections). The predictions are calculated using MSTW2008 PDF sets with the appropriate order of perturbative QCD. The uncertainty bands include the PDF and α_S variations at 68% CL, scale variations between 0.5 and 2 times the nominal scales, and the uncertainty in the PI correction. The ratios of all three theoretical predictions (solid lines) to the data are shown in the lower panels. The data (solid points) are displayed at unity with the statistical (inner) and total (outer) measurement uncertainties..

5 QCD analysis and XFitter (HERAFitter) development

A precise determination of PDFs as a function of x and Q^2 requires large amounts of experimental data that cover a wide kinematic region and that are sensitive to partonic densities of different kinds. Measurements of inclusive Neutral Current (NC) and Charge Current (CC) Deep Inelastic Scattering (DIS) at the lepton-proton (ep) collider HERA provided crucial information for determining the PDFs. Different processes in proton-proton (pp) and proton-

antiproton ($p\bar{p}$) collisions at the LHC and the Tevatron, respectively, provide complementary information to the DIS measurements.

The PDFs are determined from χ^2 fits of the theoretical predictions to the data. The HERAFitter [71], an open source project for QCD analysis of experimental data, was launched by colleagues from DESY and initially was meant for the analysis DIS results obtained at HERA experiments. With participation of the SANC group members it was subsequently extended to include proton-(anti)proton collisions measured at the LHC experiments [71, 72, 73].

The current version of the HERAFitter framework provides a set of tools for QCD analysis of pp , $p\bar{p}$ and ep scattering data, determination of PDFs and extraction of fundamental QCD parameters, such as heavy quark masses and strong coupling constant, and provides a common testing ground for theoretical models and consistency checks of the experimental results .

The diagram in Figure 18 gives a schematic overview of the HERAFitter structure and functionality, which can be divided into four main blocks:

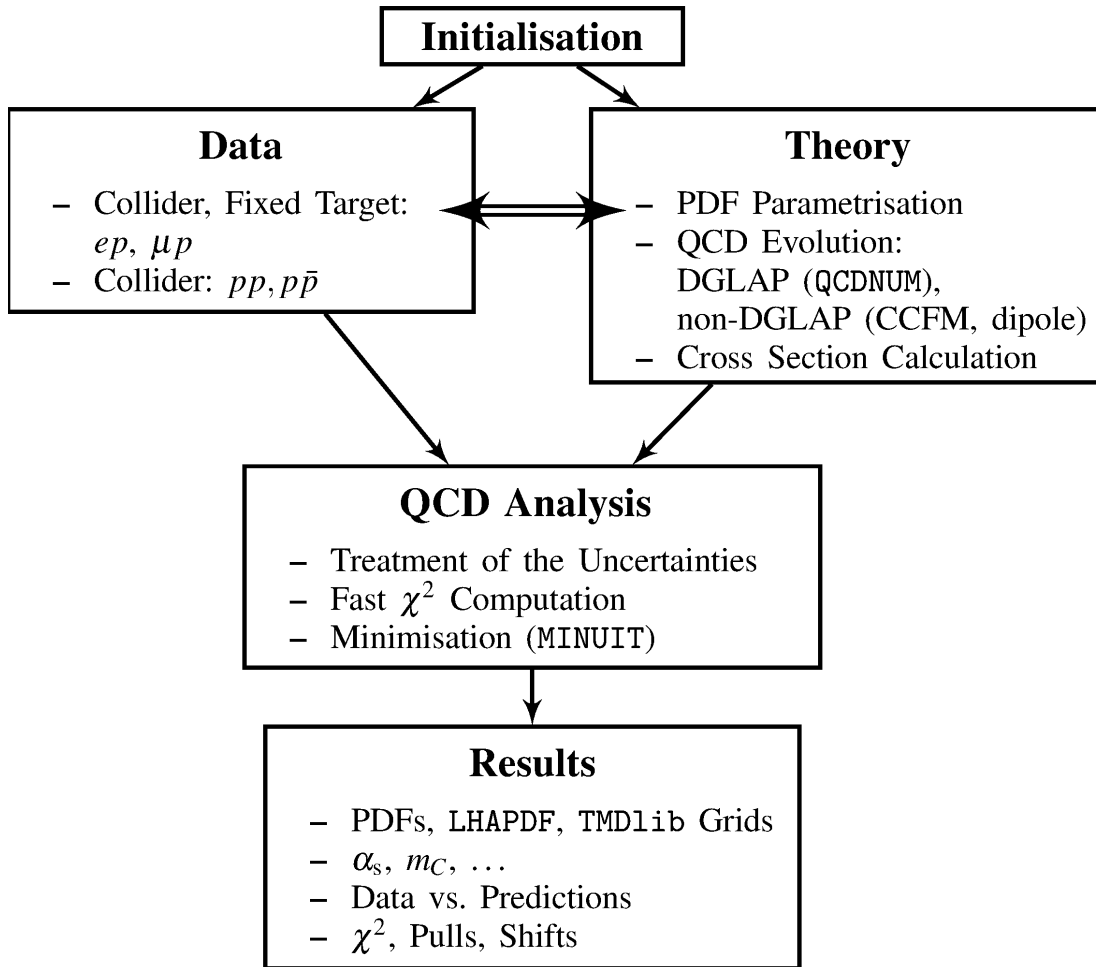


Figure 18: Schematic overview of the HERAFitter program.

Data: Measurements from various processes are provided in the HERAFitter package:

- HERA inclusive scattering data are directly sensitive to quark PDFs and indirectly sensitive to the gluon PDF through scaling violations and the longitudinal structure function F_L .
- Measurements from the fixed target experiments, the Tevatron and the LHC provide additional constraints on the gluon and quark distributions at high- x and better understanding of heavy quark distributions.

Theory: The PDFs are parametrised at a starting scale, Q_0^2 , using a functional form and a set of free parameters. These PDFs are evolved to the scale of the measurements $Q^2, Q^2 >$

Experimental Data	Process	Reaction	Theory schemes calculations
HERA, Fixed Target	DIS NC	$ep \rightarrow eX$ $\mu p \rightarrow \mu X$	TR', ACOT, ZM (QCDNUM), FFN (OPENQCDRAD, QCDNUM), TMD (uPDFevolv)
HERA	DIS CC	$ep \rightarrow \nu_e X$	ACOT, ZM (QCDNUM), FFN (OPENQCDRAD)
	DIS jets	$ep \rightarrow e \text{ jets} X$	NLOJet++ (fastNLO)
	DIS heavy quarks	$ep \rightarrow ec\bar{c}X$, $ep \rightarrow ebbX$	TR', ACOT, ZM (QCDNUM), FFN (OPENQCDRAD, QCDNUM)
Tevatron, LHC	Drell-Yan	$pp(\bar{p}) \rightarrow l\bar{l}X$, $pp(\bar{p}) \rightarrow l\nu X$	MCFM (APPLGRID)
	top pair	$pp(\bar{p}) \rightarrow t\bar{t}X$	MCFM (APPLGRID), HATHOR, DiffTop
	single top	$pp(\bar{p}) \rightarrow tl\nu X$, $pp(\bar{p}) \rightarrow tX$, $pp(\bar{p}) \rightarrow tWX$	MCFM (APPLGRID)
	jets	$pp(\bar{p}) \rightarrow \text{jets} X$	NLOJet++ (APPLGRID), NLOJet++ (fastNLO)
LHC	DY heavy quarks	$pp \rightarrow VhX$	MCFM (APPLGRID)

Table 6: The list of experimental data and theory calculations implemented in the HERAFitter package.

Q_0^2 . By default, the evolution uses the DGLAP formalism as implemented in QCDNUM [74]. The prediction of the cross section for a particular process is obtained, assuming factorisation, by the convolution of the evolved PDFs with the corresponding parton scattering cross section. Available theory calculations for each process are listed in Tab. 6.

QCD Analysis: The PDFs are determined using a χ^2 -criteria of how well theory predictions describe the input data. Various choices for the treatment of experimental uncertainties are available being implemented in the χ^2 definition.

Results: The resulting PDFs are provided in a format ready to be used by the LHAPDF library. The HERAFitter drawing tools can be used to display the PDFs with their uncertainties at a chosen scale. An example of the first set of PDFs extracted using HERAFitter

from HERA I data, HERAPDF1.0, is shown in Figure 19.

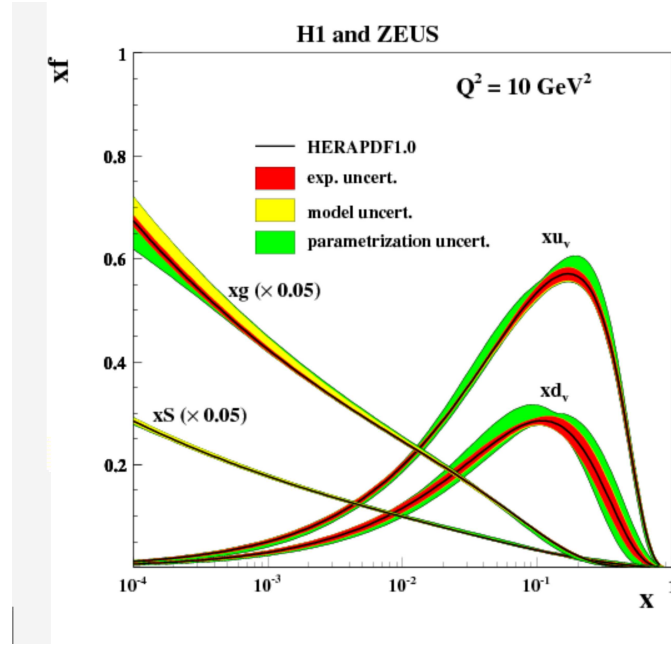


Figure 19: Distributions of valence (xu_v , xd_v), sea (xS) and the gluon (xg) PDFs in HERAPDF1.0. The gluon and the sea distributions are scaled down by a factor of 20. The experimental, model and parametrisation uncertainties are shown as coloured bands.

Corrections to the neutral current Drell-Yan cross-section due to photon-induced process $\gamma\gamma \rightarrow \ell^+\ell^-$ can reach up to 10 – 20% for high invariant mass $M_{\ell^+\ell^-}$ with the appropriate choice of kinematic cuts. Such amount makes relevant estimation of photonic PDFs in the proton using the LHC data [75], [76].

3-differential cross-section of the process $p[\gamma]p[\gamma] \rightarrow \ell^+\ell^-$ at LO reads

$$\begin{aligned} \frac{d\sigma(p[\gamma]p[\gamma] \rightarrow \ell^+\ell^-)}{dx dy dz} &= \\ &= \frac{4\pi\alpha^2}{s_0} f_\gamma \left(\frac{M_{min}}{\sqrt{s_0}} e^{x+y}, \mu_F^2 \right) f_\gamma \left(\frac{M_{min}}{\sqrt{s_0}} e^{x-y}, \mu_F^2 \right) (1 + \tanh^2 z), \end{aligned} \quad (16)$$

$$x = \ln \frac{M_{\ell^+\ell^-}}{M_{min}}, \quad y = Y_{\ell^+\ell^-}, \quad z = -\ln \tan \frac{\theta}{2}.$$

Several steps have already been made to create an infrastructure for QED analysis of the proton structure [77].

- A list of photon induced processes was implemented in the SANC Monte-Carlo generator: $\gamma + q \rightarrow q' + \ell^+ + \nu_\ell$, $\gamma + q \rightarrow q + \ell^- + \ell^+$, $\gamma\gamma \rightarrow \ell^+\ell^-$
- APPLgrid [78] interface for fast evaluation of these cross sections was created, which also required a modification of the standard APPLgrid code to account for one extra parton density (photon).

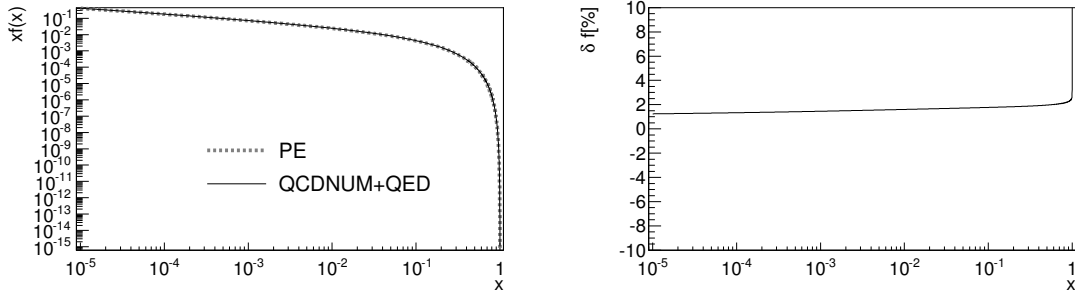


Figure 20: Tuned comparison between QCDNUM+QED and `partonevolution`. Left plot shows the momentum distribution of γ at $\mu^2 = 10^4 \text{ GeV}^2$. The corresponding δf is shown on the right plot.

- DGLAP evolution equations, and their solutions in the QCDNUM package, were enhanced with QED corrections to provide a proper treatment of photonic density in the proton.

QED-modified DGLAP evolution equations for PDF of quarks $q_i(x, \mu_F^2)$, anti-quarks $\bar{q}_i(x, \mu_F^2)$, gluon $g(x, \mu_F^2)$ and photon $\gamma(x, \mu_F^2)$ have the following form:

$$\begin{aligned}
\frac{\partial q_i}{\partial \ln \mu^2} &= \sum_{j=1}^{n_f} P_{q_i q_j} \otimes q_j + \sum_{j=1}^{n_f} P_{q_i \bar{q}_j} \otimes \bar{q}_j + P_{q_i g} \otimes g + P_{q_i \gamma} \otimes \gamma, \\
\frac{\partial \bar{q}_i}{\partial \ln \mu^2} &= \sum_{j=1}^{n_f} P_{\bar{q}_i q_j} \otimes q_j + \sum_{j=1}^{n_f} P_{\bar{q}_i \bar{q}_j} \otimes \bar{q}_j + P_{\bar{q}_i g} \otimes g + P_{\bar{q}_i \gamma} \otimes \gamma, \\
\frac{\partial g}{\partial \ln \mu^2} &= \sum_{j=1}^{n_f} P_{g q_j} \otimes q_j + \sum_{j=1}^{n_f} P_{g \bar{q}_j} \otimes \bar{q}_j + P_{g g} \otimes g, \\
\frac{\partial \gamma}{\partial \ln \mu^2} &= \sum_{j=1}^{n_f} P_{\gamma q_j} \otimes q_j + \sum_{j=1}^{n_f} P_{\gamma \bar{q}_j} \otimes \bar{q}_j + P_{\gamma \gamma} \otimes \gamma,
\end{aligned} \tag{17}$$

where \otimes -operation denotes the Mellin convolution defined as

$$[f \otimes g](x) \equiv \int_x^1 \frac{dz}{z} f\left(\frac{x}{z}\right) g(z) = \int_x^1 \frac{dz}{z} f(z) g\left(\frac{x}{z}\right), \tag{18}$$

here μ is the factorisation scale to which the densities to be evolved and P_{ab} are the splitting functions which are computed up to NNLO QCD and LO EW (see details in [77]).

The numerical results of solution of the QED-modified evolution equations were cross checked with other codes, `partonevolution` and `APFEL`, and compared to the `MRST2004QED` PDF (obsolete). Figure 20 shows good agreement of the photon density in particular with the `partonevolution` results.

6 The main objectives of the SANC group in 2018 year

The main objectives of the SANC group in 2018 are:

- Drell-Yan process analysis in the ATLAS experiment: theoretical prediction and fast differential cross section calculation using dedicated simulation tools (APPLgrid).
- Development of a computer package DYTURBO for fitting the effective sine for experiment ATLAS.
- Development and maintenance of the xFitter project. Extension of functionality, bug fixes, introduction of new experimental data and their analysis. A.Sapronov will be assigned the role of the project convener.

The main prerequisites for the undertaken studies were the expertise of participants in the field of collider phenomenology and data analysis, long history of development of theoretical basis and instruments, access to the newest experimental results and active collaboration with the international scientific community.

Talks at international meetings (2014–2018)

- R. Sadykov, CLIC, CERN, 24 January, 2018. (parallel)
- A. Sapronov, M_W WS, CERN, April, 2018. (parallel)
- A. Arbuzov, Loops and Legs, Germany, 30 April, 2018. (parallel)
- R. Sadykov, EMMI WS, Krakow, Poland, 06 September, 2017. (parallel)
- R. Sadykov, IC Modern Trends in Physics, Baku, 21.04.2017. (parallel)
- R. Sadykov, M_W WS, CERN, 28.06.2016. (parallel)
- R. Sadykov, xFitter Workshop, Dubna, Russia, 19.02.2016
- R. Sadykov, LAPP, Annecy, 22.05.2015
- R. Sadykov, ISMD2014, Bologna, Italy, September 11, 2014. (parallel)
- V. Kolesnikov, QCD@LHC2014, Suzdal, Russia, August 25-29, 2014. (parallel)

7 Conclusion

As the result, the project solved most of the planned tasks. The results obtained by the participants have been presented more than 50 publications in peer-reviewed journals and reported on the international workshops and conferences. 10 diplomas thesis were defended for a bachelor's degree and 5 Master's thesis. 6 PhD thesis were defended and 2 doctoral thesis.

All tasks of the project has successfully evaluated in close co-operation with members of the ATLAS collaboration at CERN and DESY collaboration.

References

- [1] D. Bardin, G. Passarino, L. Kalinovskaya, P. Christova, A. Andonov, S. Bondarenko, and G. Nanava, “Project ‘CalcPHEP: Calculus for precision high-energy physics’”, 2002, [hep-ph/0202004](#).
- [2] A. Andonov, D. Bardin, S. Bondarenko, P. Christova, L. Kalinovskaya, G. Nanava, and G. Passarino, *Nucl. Instrum. Meth.* **A502** (2003) 576–577.
- [3] G. Nanava, *Nucl. Instrum. Meth.* **A502** (2003) 583–585.
- [4] D. Yu. Bardin and G. Passarino, *The standard model in the making: Precision study of the electroweak interactions*. 1999.
- [5] J. A. M. Vermaseren, [math-ph/0010025](#).
- [6] D. Yu. Bardin, P. Christova, L. Kalinovskaya, and G. Passarino, *Eur. Phys. J.* **C22** (2001) 99–104, [hep-ph/0102233](#).
- [7] A. Andonov, D. Bardin, S. Bondarenko, P. Christova, L. Kalinovskaya, and G. Nanava, *Phys. Part. Nucl.* **34** (2003) 577–618, [Fiz. Elem. Chast. Atom. Yadra34,1125(2003)], [hep-ph/0207156](#).
- [8] A. B. Arbuzov, D. Yu. Bardin, and L. V. Kalinovskaya, *JHEP* **06** (2005) 078, [hep-ph/0407203](#).
- [9] A. Andonov, S. Jadach, G. Nanava, and Z. Was, *Acta Phys. Polon.* **B34** (2003) 2665–2672, [hep-ph/0212209](#).
- [10] G. Nanava and Z. Was, *Acta Phys. Polon.* **B34** (2003) 4561–4570, [hep-ph/0303260](#).
- [11] A. Andonov, A. Arbuzov, D. Bardin, S. Bondarenko, P. Christova, L. Kalinovskaya, G. Nanava, and W. von Schlippe, *Comput. Phys. Commun.* **174** (2006) 481–517, [Erratum: *Comput. Phys. Commun.*177,623(2007)], [hep-ph/0411186](#).
- [12] D. Bardin, S. Bondarenko, L. Kalinovskaya, G. Nanava, L. Romyantsev, and W. von Schlippe, *Comput. Phys. Commun.* **177** (2007) 738–756, [hep-ph/0506120](#).
- [13] A. Arbuzov, D. Bardin, S. Bondarenko, P. Christova, L. Kalinovskaya, G. Nanava, and R. Sadykov, *Eur. Phys. J.* **C46** (2006) 407–412, [Erratum: *Eur. Phys. J.*C50,505(2007)], [hep-ph/0506110](#).
- [14] R. Sadykov, A. Arbuzov, D. Bardin, S. Bondarenko, P. Christova, L. Kalinovskaya, and G. Nanava, *PoS TOP2006* (2006) 036.
- [15] A. Arbuzov, D. Bardin, S. Bondarenko, P. Christova, L. Kalinovskaya, G. Nanava, R. Sadykov, and W. von Schlippe, *Eur. Phys. J.* **C51** (2007) 585–591, [hep-ph/0703043](#).
- [16] D. Bardin, S. Bondarenko, L. Kalinovskaya, G. Nanava, and L. Romyantsev, *Eur. Phys. J.* **C52** (2007) 83–92, [hep-ph/0702115](#).

- [17] D. Bardin, L. Kalinovskaya, V. Kolesnikov, and E. Uglov, “Light-by-light scattering in SANC”, in *International School-Workshop on Calculations for Modern and Future Colliders (CALC 2006) Dubna, Russia, July 15-25, 2006*, 2006, [hep-ph/0611188](#).
- [18] A. Andonov, A. Arbuzov, S. Bondarenko, P. Christova, V. Kolesnikov, and R. Sadykov, [hep-ph/0610268](#).
- [19] A. Andonov, A. Arbuzov, S. Bondarenko, P. Christova, V. Kolesnikov, and R. Sadykov, *Phys. Part. Nucl. Lett.* **4** (2007) 451–460.
- [20] D. Bardin, S. Bondarenko, L. Kalinovskaya, G. Nanava, L. Romyantsev, and W. von Schlippe, *Eur. Phys. J.* **C54** (2008) 187–197, [0710.3083](#).
- [21] A. Andonov, A. Arbuzov, S. Bondarenko, P. Christova, V. Kolesnikov, G. Nanava, and R. Sadykov, *Phys. Atom. Nucl.* **73** (2010) 1761–1769, [0901.2785](#).
- [22] A. Arbuzov, D. Bardin, S. Bondarenko, P. Christova, L. Kalinovskaya, G. Nanava, and R. Sadykov, *Eur. Phys. J.* **C54** (2008) 451–460, [0711.0625](#).
- [23] A. Arbuzov, A. Andonov, D. Bardin, S. Bondarenko, P. Christova, L. Kalinovskaya, V. Kolesnikov, G. Nanava, and R. Sadykov, *PoS ACAT08* (2008) 109.
- [24] D. Bardin, L. Kalinovskaya, and E. Uglov, *Phys. Atom. Nucl.* **73** (2010) 1878–1888, [0911.5634](#).
- [25] D. Y. Bardin, L. Kalinovskaya, and E. Uglov, *Phys. Atom. Nucl.* **76** (2013) 1339–1344, [1212.3105](#).
- [26] D. Bardin, S. Bondarenko, P. Christova, L. Kalinovskaya, W. von Schlippe, and E. Uglov, *Phys. Part. Nucl. Lett.* **14** (2017), no. 6 811–816, [1709.05978](#).
- [27] A. B. Arbuzov and R. R. Sadykov, *J. Exp. Theor. Phys.* **106** (2008) 488–494, [0707.0423](#).
- [28] A. Arbuzov, R. Sadykov, and Z. Was, *Eur. Phys. J.* **C73** (2013), no. 11 2625, [1212.6783](#).
- [29] S. Antropov, A. Arbuzov, R. Sadykov, and Z. Was, *Acta Phys. Polon.* **B48** (2017) 1469, [1706.05571](#).
- [30] S. G. Bondarenko and A. A. Sapronov, *Comput. Phys. Commun.* **184** (2013) 2343–2350, [1301.3687](#).
- [31] A. Arbuzov, D. Bardin, S. Bondarenko, P. Christova, L. Kalinovskaya, U. Klein, V. Kolesnikov, L. Romyantsev, R. Sadykov, and A. Sapronov, *JETP Lett.* **103** (2016), no. 2 131–136, [1509.03052](#).
- [32] A. Arbuzov, D. Bardin, S. Bondarenko, P. Christova, L. Kalinovskaya, R. Sadykov, A. Sapronov, and T. Riemann, *J. Phys. Conf. Ser.* **762** (2016), no. 1 012062.
- [33] D. Bardin, S. Bondarenko, P. Christova, L. Kalinovskaya, L. Romyantsev, A. Sapronov, and W. von Schlippe, *JETP Lett.* **96** (2012) 285–289, [1207.4400](#).

- [34] ATLAS Collaboration, G. Aad *et al.*, *Phys.Lett.* **B725** (2013) 223–242, 1305.4192.
- [35] ATLAS Collaboration, G. Aad *et al.*, *JHEP* **1406** (2014) 112, 1404.1212.
- [36] C. Buttar *et al.*, “Les houches physics at TeV colliders 2005, standard model and Higgs working group: Summary report”, in *Physics at TeV colliders. Proceedings, Workshop, Les Houches, France, May 2-20, 2005*, 2006, hep-ph/0604120.
- [37] Electroweak Working Group, TeV4LHC-Top Collaboration, C. E. Gerber *et al.*, “Tevatron-for-LHC Report: Top and Electroweak Physics”, 2007, 0705.3251.
- [38] S. Alioli *et al.*, *Eur. Phys. J.* **C77** (2017), no. 5 280, 1606.02330.
- [39] F. Yuasa *et al.*, *Prog. Theor. Phys. Suppl.* **138** (2000) 18–23, hep-ph/0007053.
- [40] CompHEP Collaboration, E. Boos, V. Bunichev, M. Dubinin, L. Dudko, V. Ilyin, A. Kryukov, V. Edneral, V. Savrin, A. Semenov, and A. Sherstnev, *Nucl. Instrum. Meth.* **A534** (2004) 250–259, hep-ph/0403113.
- [41] E. Barberio and Z. Was, *Comput. Phys. Commun.* **79** (1994) 291–308.
- [42] P. Golonka and Z. Was, *Eur. Phys. J.* **C45** (2006) 97–107, hep-ph/0506026.
- [43] T. Sjostrand, S. Mrenna, and P. Z. Skands, *JHEP* **05** (2006) 026, hep-ph/0603175.
- [44] C. M. Carloni Calame, G. Montagna, O. Nicrosini, and M. Treccani, *Phys. Rev.* **D69** (2004) 037301, hep-ph/0303102.
- [45] C. M. Carloni Calame, G. Montagna, O. Nicrosini, and A. Vicini, *JHEP* **12** (2006) 016, hep-ph/0609170.
- [46] U. Baur, S. Keller, and D. Wackerroth, *Phys. Rev.* **D59** (1999) 013002, hep-ph/9807417.
- [47] U. Baur and D. Wackerroth, *Phys. Rev.* **D70** (2004) 073015, hep-ph/0405191.
- [48] U. Baur, S. Keller, and W. K. Sakumoto, *Phys. Rev.* **D57** (1998) 199–215, hep-ph/9707301.
- [49] U. Baur, O. Brein, W. Hollik, C. Schappacher, and D. Wackerroth, *Phys. Rev.* **D65** (2002) 033007, hep-ph/0108274.
- [50] S. Dittmaier and M. Krämer, *Phys. Rev.* **D65** (2002) 073007, hep-ph/0109062.
- [51] J. Kublbeck, M. Böhm, and A. Denner, *Comput. Phys. Commun.* **60** (1990) 165–180.
- [52] T. Hahn and J. I. Illana, *Nucl. Phys. Proc. Suppl.* **160** (2006) 101–105, [101(2006)], hep-ph/0607049.
- [53] G. Belanger, F. Boudjema, J. Fujimoto, T. Ishikawa, T. Kaneko, K. Kato, and Y. Shimizu, *Phys. Rept.* **430** (2006) 117–209, hep-ph/0308080.

- [54] D. Bardin, S. Bondarenko, P. Christova, L. Kalinovskaya, V. Kolesnikov, and W. von Schlippe, *Phys. Part. Nucl. Lett.* **7** (2010) 72–79, 0903.1533.
- [55] D. Bardin, S. Bondarenko, L. Kalinovskaya, V. Kolesnikov, and W. von Schlippe, *Eur. Phys. J.* **C71** (2011) 1533, 1008.1859.
- [56] D. Bardin, S. Bondarenko, P. Christova, L. Kalinovskaya, V. Kolesnikov, W. von Schlippe, K. Yordanova, and K. Yordanova, *Phys. Part. Nucl. Lett.* **9** (2012) 472–483, 1110.3622.
- [57] D. Bardin, L. Kalinovskaya, V. Kolesnikov, and W. von Schlippe, *Phys. Atom. Nucl.* **73** (2010) 2048–2063, 0912.3893.
- [58] D. Yu. Bardin, L. V. Kalinovskaya, and L. A. Rumyantsev, *Phys. Part. Nucl. Lett.* **6** (2009) 30–41, [Pisma Fiz. Elem. Chast. Atom. Yadra2009,no.149,54(2009)].
- [59] D. Yu. Bardin, L. V. Kalinovskaya, E. D. Uglov, and W. von Schlippe, *Phys. Atom. Nucl.* **79** (2016), no. 1 95–107, [Yad. Fiz.79,no.1,37(2016)], 1411.6845.
- [60] A. Denner and T. Sack, *Nucl. Phys.* **B306** (1988) 221–238.
- [61] A. Djouadi, V. Driesen, W. Hollik, and J. Rosiek, *Nucl. Phys.* **B491** (1997) 68–102, hep-ph/9609420.
- [62] E. Gabrielli, V. A. Ilyin, and B. Mele, *Phys. Rev.* **D56** (1997) 5945–5961, [Erratum: *Phys. Rev.*D58,119902(1998)], hep-ph/9702414.
- [63] A. Denner and S. Dittmaier, *Nucl. Phys.* **B398** (1993) 265–284.
- [64] A. Denner, J. Kublbeck, R. Mertig, and M. Bohm, *Z. Phys.* **C56** (1992) 261–272.
- [65] A. Bredenstein, A. Denner, S. Dittmaier, and M. M. Weber, *Phys. Rev.* **D74** (2006) 013004, hep-ph/0604011.
- [66] A. Bredenstein, A. Denner, S. Dittmaier, and M. M. Weber, *Nucl. Phys. Proc. Suppl.* **157** (2006) 63–67, [,63(2006)].
- [67] ATLAS Collaboration, G. Aad *et al.*, *Phys.Rev.* **D85** (2012) 072004, 1109.5141.
- [68] ATLAS Collaboration, G. Aad *et al.*, *Phys.Rev.Lett.* **109** (2012) 012001, 1203.4051.
- [69] J. Butterworth, G. Dissertori, S. Dittmaier, D. de Florian, N. Glover, *et al.*, 1405.1067.
- [70] ATLAS Collaboration, G. Aad *et al.*, *Phys.Rev.* **D90** (2014), no. 5 052005, 1405.4123.
- [71] S. Alekhin, O. Behnke, P. Belov, S. Borroni, M. Botje, *et al.*, 1410.4412.
- [72] HERAFitter developers’ team Collaboration, P. Belov *et al.*, *Eur.Phys.J.* **C74** (2014), no. 10 3039, 1404.4234.
- [73] HERAFitter developers’ Team Collaboration, S. Camarda *et al.*, 1503.05221.

- [74] M. Botje, *Comput.Phys.Commun.* **182** (2011) 490–532, 1005.1481.
- [75] analysis team Collaboration, F. Giuli, *PoS EPS-HEP2017* (2017) 375, 1708.03623.
- [76] xFitter Developers' Team Collaboration, F. Giuli *et al.*, *Eur. Phys. J.* **C77** (2017), no. 6 400, 1701.08553.
- [77] R. Sadykov, 1401.1133.
- [78] T. Carli, D. Clements, A. Cooper-Sarkar, C. Gwenlan, G. P. Salam, *et al.*, *Eur.Phys.J.* **C66** (2010) 503–524, 0911.2985.